ACS APPLIED MATERIALS & INTERFACES

Biological and Medical Applications of Materials and Interfaces

A multifunctional lipid incorporating active targeting and dual-control release capabilities for precision drug delivery

Chenyu Liu, Kai K Ewert, Weihe Yao, Ning Wang, Youli Li, Cyrus R Safinya, and Weihong Qiao

ACS Appl. Mater. Interfaces, **Just Accepted Manuscript** • DOI: 10.1021/acsami.9b14470 • Publication Date (Web): 27 Nov 2019

Just Accepted

is published by the American Chemical Society. 1155 Sixteenth Street N.W., Washington, DC 20036

A multifunctional lipid incorporating active targeting and dual-control release capabilities for precision drug delivery

Chenyu Liu[1,2], Kai K. Ewert[2], Weihe Yao[1], Ning Wang[1], Youli Li[3], Cyrus R. Safinya[2]*, Weihong Qiao[1]*

[1] State Key Laboratory of Fine Chemicals, School of Chemical Engineering, Dalian University of Technology, Dalian, 116024, P. R. China

[2] Materials, Physics, and Molecular, Cellular & Developmental Biology Departments, University of California at Santa Barbara, California 93106, USA

[3] Materials Research Laboratory, University of California at Santa Barbara, California 93106, USA

*Corresponding authors contact information:

Safinya@mrl.ucsb.edu

qiaoweihong@dlut.edu.cn

TOC graphic

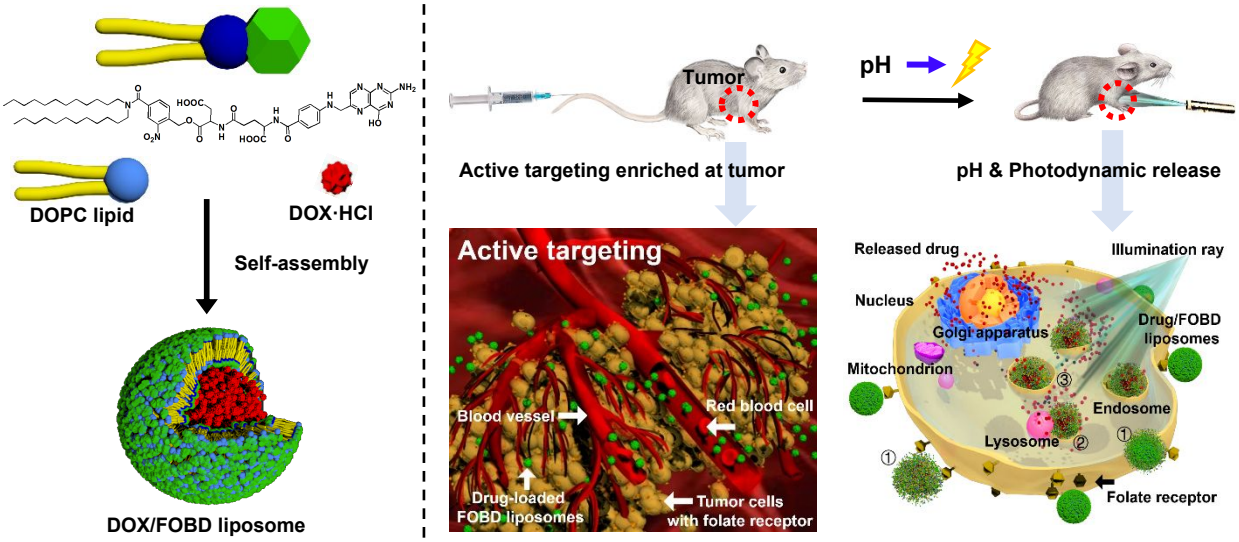

Abstract

Active targeting and precise control of drug release based on nanoparticle-based therapies are urgently required to precisely treat cancer. We have custom synthesized a functional lipid (termed Fa-ONB) by introducing a folic acid targeting group into an *o*-nitro-benzyl ester lipid. As designed, the liposomes formed by Fa-ONB combine active targeting and dual trigger release capabilities, which help to improve drug efficacy and reduce the toxicity of traditional liposomes. We first verified that both pH-induced hydrolysis and light treatment were able to cleave Fa-ONB lipid. We then prepared a series of liposomes (termed FOBD liposomes) by compounding the Fa-ONB lipid with DOPC at different ratios. After encapsulation of doxorubicin (DOX), we found that the particle size of DOX-loaded FOBD liposomes (DOX/FOBD) first increased (290 nm to 700 nm) and then decreased again (to 400 nm) under continuous UV irradiation (120 min). The photocatalytic release efficiency under different pH conditions was investigated by dialysis experiments, and it was found that the release efficiency in an acidic environment was significantly increased relative to neutral pH. This pH-triggered release response helps distinguish pathological tissues such as lysosomal compartments and tumors. The light-induced formation of a DOX precipitate increases in efficiency with increasing UV exposure time as well as with increasing environmental acidity or alkalinity. In addition, confocal imaging and flow cytometry showed that the ability of FOBD lipids to actively target HeLa cells increased with increasing Fa-ONB lipid content. Real-time *in vivo* fluorescence small animal experiments proved targeting to tumors and pH- and photo-induced release properties. Furthermore, therapeutic experiments using a mouse model found significant tumor inhibitory effect for DOX/FOBD55 liposomes with UV irradiation, clearly demonstrating the benefit of light treatment: the tumor size of the control (PBS) group was 7.59 times that of the light treatment group. Therefore, this research demonstrates the benefits of combining triggerable release functions and effective active tumor targeting in one small lipid molecule for precise cancer treatment.

Keywords

Cancer therapy, Nanoparticles, Folate-targeted drug delivery, O-nitrobenzyl, Dual-control release

1. Introduction

Cancer is a major disease that threatens human life and millions of people are diagnosed with this disease every year.[1] At present, chemotherapy is still the most applied clinical treatment together with surgery and radiotherapy, but it has many shortcomings, such as the non-specific distribution of anticancer drugs, which often causes side effects on other tissues (e.g. myelosuppression, cardiomyopathy, and neurotoxicity).[2] Moreover, the anti-tumor drugs commonly used in clinical practice generally lack selectivity to tumor tissues[3] and a significant quantity of them will be devoured by the lymphatic system, necessitating increasing the dosage of drug with inescapable damage on the immune system. The lack of techniques to responsibly regulate treatment, and multi-drug resistance make the present clinical treatment unsatisfactory. Nano-drug-carrier technology is one of the promising directions of nanobiotechnology for modern pharmacy.[4] The drug is encapsulated in or adsorbed on the surface of submicrometer-size particles that could desirably regulate the release rate, increase the permeability of biological barriers, change the distribution of drug *in vivo* or improve the bioavailability of drugs.[5, 6] Research in the field of medical applications is still in its infancy, and its application prospects are broad.[7]

In order to reduce the toxicity and improve the efficacy simultaneously, tumor-targeted nanomedicine therapy that selectively destroys tumor tissue has become the dominant direction of cancer therapy.[8] Compared to an active targeting vector system that utilizes antigen/antibody or ligand/receptor specific binding to achieve targeted drug delivery, conventional liposome-based passive targeting (EPR) drug delivery lacks an active recognition process, thus leading to poor therapeutic efficacy.[9-11] Because of their relatively straightforward process of synthesis, separation and purification and favorable biosafety properties, small molecule targeting moieties are widely applied to active targeted therapy.[12-14] In most targets, folic acid and its derivatives[15-20] is a natural ligand for folate receptors and can be reduced to tetrahydrofolate for participating in the metabolism. Many epidemiological and clinical studies have shown that folic acid has preventive effects on colon, lung, pancreatic, esophageal, cervical cancers etc. and the lack of folate can lead to hypomethylation of genomic DNA and hypermethylation of

specific sites within the nucleotide, thereby causing tumorigenesis. Therefore, it is generally believed that supplementing folic acid helps inhibit cancer.[21] Studies have found that under physiological conditions, folate receptors are expressed at low levels in the lung, thymus, kidney, choroid plexus, and placenta. However, the expression of folate receptors in malignant cell lines is 20 to 200 times higher than in normal cell lines.[22, 23] The expression level of folate receptor is not only positively correlated with the malignant degree and metastatic invasiveness of tumor tissues, but also express higher in metastatic tumors than in in-situ tumors.[24] Therefore, the introduction of folic acid into the liposomal lipid for drug deliver can be beneficial in many aspects, including targeting specific cancer cells, treating diffuse cancer and supplementing the human body during the treatment.

In addition to enhanced aggregation of drug delivery particles on the targeted cells, effective release of the drug is crucial to successful delivery. Considering that most anticancer drugs need to transfer into the nucleus and combine with certain specific parts of DNA to inhibit a gene's transcriptional activity,[25-28] the low efficacy of many (even targeted) drug-loaded liposomes, i.e., of the fraction of liposomes which have bypassed the major barriers of macrophage/immune system clearance and uptake by the liver and have reached the tumor, may be related to their inability to transfer into the nucleus effectively. As the specific extracellular environment of tumor tissue is weakly acidic (pH 6.0-6.8, strong anaerobic metabolism), and the pH value of intracellular organelles involved in liposome metabolism is even lower (such as lysosome, pH 4.0-6.0), pH-sensitive lipids that can react to this endogenous stimulus are good candidates for controlled release. However, most of the single pH-triggered liposomes currently reported only promote the release efficiency around 20%.[29-33] Additionally, diffused cancer cells cause pH environments indistinguishable from normal tissue, which limits the effectiveness of pH-regulated release from liposomes. Thus, it would be very difficult for a single-reaction drug delivery system to meet the requirement of automatically regulated release.[34, 35]

Photo-induced release (exogenous stimulation) has advantages in high local precision, convenient triggering conditions, precise manual regulation release, and small damage to

healthy tissues.[36-40] To this end, combining a photo-controlled dissociable part with a pH-triggered cleavable site could provide additional ability to modulate the drug release process. The *o*-nitrobenzyl ester bond can be dissociated under acidic or alkaline conditions and can also be easily photolyzed by ultraviolet light (Norrish Type II intramolecular rearrangement).[41] Moreover, the micelles formed with *o*-nitrobenzyl groups can be light-decomposed by absorption of two NIR photons under near-infrared (NIR) light conditions.[42-47] This highly expands the use of *o*-nitrobenzyl compounds as human tissue can transparent more NIR light than UV light. Alternatively, upconverting nanoparticles (UCNPs, anti-Stokes materials) can be packaged into nanoparticles to circumvent the weak tissue penetration of UV light.[48-51] Therefore, the *o*-nitrobenzyl ester moiety is one of the simplest structures that can realize two major control methods (pH and photo sensitivity) simultaneously. We hypothesized that a suitable *o*-nitrobenzyl ester derivative could promote pH-induced initial release of its drug cargo which could then be enhanced more precisely and manually with tailored light therapy conditions to locally release the additional drug.

Here, we propose a new method for combining active targeting with dual triggering release abilities in one single lipid (termed Fa-ONB) for creating a precise drug carrier. The lipid is designed with multifunction features: the two lipid tails in the molecule allow for liposome formation,[52, 53] the *o*-nitrobenzyl ester enable dual (pH and light) triggering reactions, and the folate moiety actively targets cancer cells. As shown in Scheme 1a and b, by compounding with DOPC lipids, the surface of the drug-loaded liposomes (abbreviated as drug-loaded FOBD liposomes) were uniformly covered by folic acid moieties, which led to active enrichment at tumor cells after injection into a tumor mouse model. In addition, under the stimulation of the acidic intracellular or extracellular environment of the tumor site, the FOBD liposomes initially release the loaded drug. Subsequently, controlled phototherapy could be employed to release additional drugs.

The Fa-ONB lipid was synthesized by conjugating activated folic acid to a lipid scaffold prepared from 4-(bromomethyl)-3-nitro-benzoic acid and didodecylamine. After verifying the sensitivity of the Fa-ONB lipid to pH- and light-triggered cleavage at the molecular level, a series of FOBD liposomes (compounded with different proportions of DOPC lipids) were

prepared. The drug doxorubicin (DOX; commonly used for chemotherapy) was selected as the encapsulated drug, and the triggering characteristics and cytotoxicity of the series of FOBD and DOX/FOBD liposomes were evaluated. Subsequently, we used flow cytometry, confocal imaging, and small animal fluorescence imaging systems to verify the active targeting and dual-triggered drug release of DOX/FOBD liposomes. Based on their tumor actively targeting ability, encapsulation efficiency and controlled release characteristics, we chose FOBD55 liposomes as the composition to study its therapeutic effect in a mouse model. The UV light was used to induce the photolysis of DOX/FOBD55 liposomes in the subcutaneous tumors, and it was found that the phototherapy group most inhibited tumor growth.

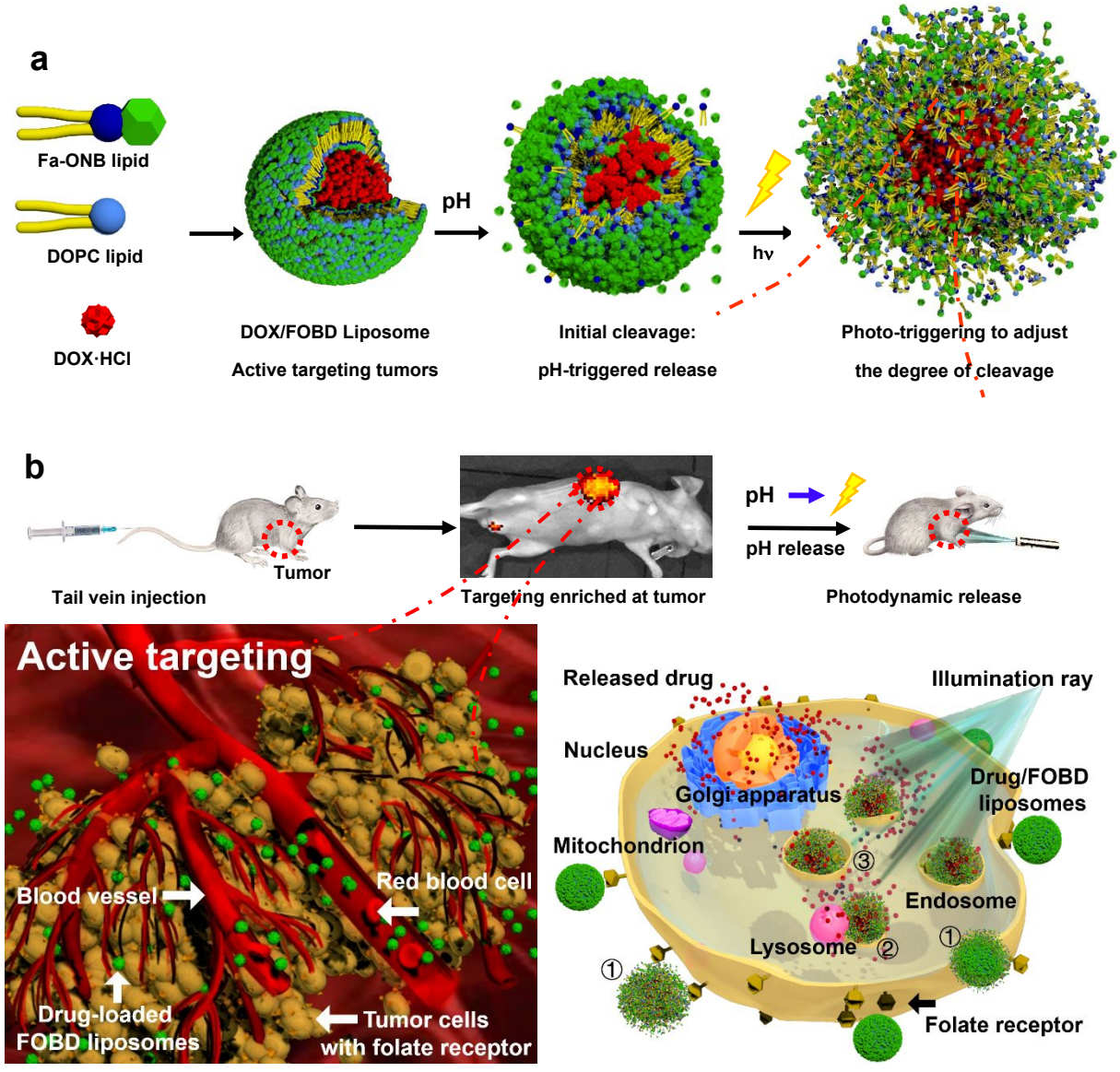

Scheme 1. Schematic depiction of FOBD liposomes for active targeting and controlled drug release. (a) Fa-ONB lipids compounded with DOPC lipids to encapsulate DOX (doxorubicin hydrochloride, DOX·HCl) for preparing drug-loaded FOBD (DOX/FOBD) liposomes. Active targeting of the tumor cells is achieved because the entire surface of the FOBD liposome is uniformly covered by the folic acid target. In a tumor or intracellular environment (low pH acidic environment), the o-nitrobenzyl ester bond of the FOBD liposome could be partially dissociated with a small amount of drug release. Lately, the degree of release can be controlled by adjusting the illumination conditions for an additional light-triggered release. (b) The overview of using FOBD liposomes for cancer treatment. The drug loaded FOBD liposomes are actively targeting and enriched at the tumor sites after being injected into a tumor mouse model (detection by animal fluorescence system). The external acidic environment of the tumor will stimulate the initial release of the drug-loaded liposomes (and drug transfers into the cell due to the concentration gradient between the outside and inside of the cell (①)). Most of the DOX/FOBD liposomes quickly enter the cell by active transport. A portion of these internalized liposomes are cleaved by the action of acidic lysosomes. This release of free DOX inside the cell establishes a DOX concentration gradient between nucleus and cytoplasm, and this gradient (which is enhanced by the interaction of DOX with DNA in the nucleus) drives free DOX transfer to the nucleus (②). (Only the released free DOX can transfer to the nucleus because liposomes are not small enough to pass through the nuclear pores.) Meanwhile, by irradiating the tumor site, with the pH stimulation, the DOX/FOBD liposomes could release additional drug from endocytosed, thereby accelerating the transfer of drug to the nucleus (③).

2. Experimental Section

2.1 Photolysis properties of Fa-ONB lipids

The Fa-ONB lipid was dissolved in DMF and divided into 12 portions (in closed quartz cell). These samples were irradiated under UV light (365 nm, 60 W) for 0, 5, 15, 30, 45, 60, 70, 80, 90, 100, 110 and 120 min. After irradiation, UV, IR (0, 5, 60, 120 min) and TLC [54] were used to judge the degree of light-cleavage, and mass spectrometry was performed to identify the compounds generated after illumination.

2.2 pH-sensitive properties of Fa-ONB lipids

Dissolve an equal amount of Fa-ONB lipid in an equal volume of buffer at different pH (phosphate, pH=4.2, 6.5, 7.4, 8.0 and 8.5). Stir at room temperature for 30 minutes, then analyze the compound samples by TLC, IR (pH = 6.5 and pH = 8.5) and MS. The new generated product was separated by silica gel chromatography, and then MS, and NMR were used for charactering the resulting colorless oil. [54]

2.3 Buffering capacity of Fa-ONB lipid

The Fa-ONB lipid was dissolved in deionized water to obtain a 40 mL of 1 mM solution. The solution was divided into two portions, and the pH values of these two solutions were adjusted with 0.01 mM HCl and 0.01 mM NaOH, respectively. The volume of the dropping acid or alkali and the pH of the solution were compared to the pH buffering capacity of saturated NaCl solution.

2.4 Preparation of FOBD liposomes

787.6 mg of DOPC lipid and 106.9 mg of Fa-ONB lipid were separately dissolved in 10 mL of chloroform/methanol (1:1, v/v) to prepare two 10 mM stock solutions. The prepared stock solutions were mixed at a ratio of 10:0, 7:3, 5:5, 3:7, and 0:10 to prepare a series of FOBD liposome samples (e.g., composite lipid with Fa-ONB/DOPC equals 7:3 was named FOBD73). The solvent was evaporated under nitrogen and dried in vacuum at 30 ° C for 12 h, and then 4 mL of PBS (0.01 M) was added to configure a 0.25 mM sample. The mixture was incubated for an additional 24 hours at 37 °C, then ultrasonicated to obtain uniformly dispersed liposomes (FOBD). (15 min, power 50%, ultrasonic 3 s, intermittent 10 s).

2.5 Characterization and pH-based photolysis behavior of empty FOBD liposomes

For studying liposome stability, samples of sonicated FOBD55 liposomes were selected as a representative sample to incubate in the dark environment for 15 days and the Malvern Zetasizer Nano ZS was used to measure the particle size of it. Aliquots of a 0.25 mM empty FOBD73, FOBD55 and FOBD37 liposomes were separately prepared in phosphate buffer with different pH (4.2, 6.5, 7.4 and 8.5) and irradiated with 0, 5, 10, 20, 30, 60, 90 and 120 min to assess the effects of light irradiation and pH triggering on liposomes.[54] The degree of

dissociation of FOBD liposomes under different pH and light conditions were observed by UV spectrum. The Malvern Zetasizer Nano ZS was used to measure the size distribution and hydrodynamic diameter of the empty FOBD liposomes. Serval light exposed 30 μL of FOBD55 samples (0, 10, and 60 min) were placed on copper grids for getting transmission electron microscopy imaging (TEM, HT7700 EXALENS electron microscope).

2.6 Encapsulation efficiency of DOX/FOBD at different lipid/drug ratios

Varying amounts of DOPC and Fa-ONB stock solution at the ratio of 10:0, 7:3, 5:5, 3:7 and 0:10 were evaporated under nitrogen. After drying overnight, a stock solution of 10 mM DOX·HCl in PBS (pH=7.4, 0.01 M) was added in each sample with a lipid/drug ratio at 3:1.[54] The ultrasonicated solutions were incubated for 24 h at 37 °C , transferred to dialysis bags (MW cutoff=1000) and then immersed in 600 mL PBS. Exchange the PBS solution every 0.5 h for 4 h. After that, the solvent (water) in each sample was freeze-dried, and the DOX encapsulation efficiency of each sample was tested by the UV spectrum (in DMF, referring to the standard curve of free DOX).

2.7 Photolysis ability of DOX / FOBD liposomes

Considering the drug encapsulation rate, samples of DOX/FOBD73, DOX/FOBD55, DOX/FOBD37 liposome solution were chosen (encapsulation rate is around 55%) and irradiated for 0, 5, 10, 20, 30, 45, 60, 75, 90, and 120 min. Malvern Zetasizer and TEM [54] were used to assess the size distribution, hydrodynamic diameter and morphological changes of DOX/FOBD55 liposomes.

2.8 Photo-release ability of pH-based DOX/FOBD liposomes

For simulating the pH and photo-controlled release ability of DOX/FOBD73, DOX/FOBD55, DOX/FOBD37 liposomes *in vivo*, we prepared a 0.25 mM DOX/FOBD liposome in PBS (pH=7.4),[54] and divided it into 3 equal parts. A 365 nm wavelength UV light (60 W) was used for irradiating liposomes solution (samples were collected at 0, 10, 30, and 60 mi). Then divided each collected sample in quadruplicate, and dialyzed them in 100 mL of phosphate buffer with different pH values (pH = 4.2, 6.5, 7.4 and 8.5). The dialysis was continued for 72

h, and the cumulative release curve of DOX was plotted by fluorescence spectroscopy.[54]

2.9 Cytotoxicity of FOBD and DOPC liposomes

Raw 264.7 macrophages, Hela7702, MCF-7 and HepG2 cells were seeded in 96-well plates (approximately 10^5 cells/mL) and placed in an incubator (37 °C, 5% CO_2 atmosphere). A total of 100 μL of fresh medium containing 20 μL of FOBD73, FOBD55, FOBD37, DOPC empty liposome suspensions (at 1.8 mM, 0.9 mM, 0.45 mM, 0.225 mM, 0.112 mM, 0.056 mM, 0.028 mM, 0.014 mM) was added when the cells had reached about 80% confluence. Aspirating the medium after cells were incubated for 24 h (in the incubator, 37 °C, 5% CO_2 atmosphere), and then washed the cells three times with fresh PBS buffer. After that, cell survival was obtained by adding MTT (solution, 0.5 mg/mL). [54]

2.10 Cytotoxicity of DOX/FOBD liposomes

Raw 264.7 macrophages, Hela7702, MCF-7 and HepG2 cells were seeded as described above (2.9), and then a total of 100 μL of medium containing 20 μL of a 0.25 mM suspension of DOX/FOBD73, DOX/FOBD55, or DOX/FOBD37 liposomes (same encapsulation rate, around 55%) was added. Untreated control cells and treated cells were exposed under ultraviolet light for 0, 5, 10 and 20 min. To compare the cytotoxicity, we set another two groups of cells, respectively treated with free DOX and DOX/DOPC liposomes (equal amount of DOX to the FOBD liposome suspensions). The cell viability was measured as described above (MTT).

2.11 Targeting ability and photolysis ability of DOX/FOBD liposomes in cell

MCF-7 and Hela7702 were seeded in 6-well plates (10^6 cells/mL) and then were incubated with 2000 μL of fresh medium containing 500 μL of free DOX, DOX/FOBD73, DOX/FOBD55, DOX/FOBD37, DOX/DOPC and pre-irradiated 5 min of DOX/FOBD55 liposome suspensions (equal amounts of DOX, 0.25 mM of liposomes) for 90 min. After that, for each well, the medium was aspirated and replaced with fresh PBS, and then a total of 200 μL of a 0.03% (w/v) EDTA and 0.25% (w/v) trypsin solution was added to dissociated cells for 15-20 seconds. We next centrifuged the suspensions 3 min at 1000 × g, washed them twice

with PBS, re-suspended each sample in 500 μL PBS, and recorded the fluorescence histograms immediately by a flow cytometer (Thermo Fisher Scientific Attune NxT, 10,000 gated events, based on DOX fluorescence).

2.12 Direct visualization of the internalization of DOX-loaded FOBD liposomes

Hela cells were added in three 35-mm culture dishes (10^5 cells/mL) and cultured in an incubator for 12 h. The cell culture medium in each dish was refreshed (1 mL of medium), and a total of 250 μL of prepared above suspension (2.11) of free DOX, DOX/DOPC, DOX/FOBD55 and pre-irradiated (5 min) DOX/FOBD55 liposomes were respectively added to the culture dish. After incubation for 90 min, cells were washed with PBS, stained with 4% poly(oxymethylene) for 30 min, fixed with DAPI dye for 15 min, then dyed with DIO for 30 min. In the end, we washed the cells three times with PBS and then observe the fluorescence images of cells under the confocal microscope (OLYMPUS, FV1000).

2.13 Cancer treatment in a human cervical tumor mouse model

All animal experiments were performed in accordance with the guidelines of the National Institutes of Health and approved by the Animal Ethics Committee of Dalian University of Technology.

Human cervical cancer cells (Hela-7702; 5×10^7 cells/mL) were used to construct tumor mouse models.[54] After the average tumor size of mice was reached approximately 95 mm^3. The mice were randomly divided into 5 groups: control group (received PBS); DOX group (injected with free DOX solution); DOX/DOPC group (received DOX/DOPC liposomes); DOX/FOBD55 group (injected with DOX/FOBD55 liposomes); DOX/FOBD55-UV group (after injection of DOX/FOBD55 liposomes about 120 min, the tumor site was intermittently exposed under UV light for 10 min (for each time, 2 min on, 5 min off)). Every two days, injected the drug (DOX dose 2.5 mg/kg, via tail vein) and recorded the body weight and tumor size[55-57] for evaluating the effect of the therapies. The liver, spleen, heart, kidney, lung, and tumor tissues of mice were stained (hematoxylin-eosin) at the end of the treatment for evaluating systemic toxicity by an inverted microscope.[58, 59] Furthermore, in the tumor tissues, the distribution of DOX (green fluorescence) was observed by confocal microscopy (OLYMPUS, FV1000).[60]

2.14 Real-time *in vivo* fluorescence imaging of mice

We performed DOX/FOBD55, DOX/FOBD55-UV and DOX/DOPC groups to verify the tumor targeting abilities and dual-triggered control release capabilities of FOBD55 liposomes (the treatment was described as above (2.13)). Berthold LB983NC100 (real-time *in vivo* imaging system) was used for monition the fluorescence of DOX.[54, 61, 62] At injection of 24 h, the major organs and tumors of the sacrificed mice were collected and imaged to evaluate the active targetable capability and the biodistribution of DOX/FOBD liposomes.[54, 63-65]

3. Results and Discussion

3.1. Design and synthesis of the active targeting, dual-responsive Fa-ONB lipid

In order to achieve precision therapy and prevent the indiscriminate release phenomena in normal tissues, especially to reduce the drug toxicity and side effects, we designed a liposome with highly targeted and dual-trigger induced release functions. The introduction of two hydrophobic chains enables lipids to self-assemble in water and form liposomes for the encapsulation of therapeutic drugs. The folic acid is chemically integrated into the lipid so that the liposomes can actively target the tumor cell *in vivo*. The *o*-nitrobenzyl ester bond, as a controlling moiety to incorporate pH- and light-responsiveness, is the key aspect of the design, because it combines the targeting and controllable release functions in one simple structure. In the design, tumor-targeted liposomes initially dissociate by the endogenous pH trigger, and light is used as an external trigger to achieve a more accurate multistage release response allowing for accommodating the differences in lesion severity by changing the light intensity, illumination time or wavelength.[66, 67]

Scheme 2 shows the detailed synthetic route for the Fa-ONB lipid. Firstly, 4-(bromomethyl)-3-nitrobenzoic acid was coupled with didodecylamine by amidation to introduce the hydrophobic moiety. Then, through the nucleophilic substitution of the carboxyl group in Boc-Asp(O-allyl)-OH, the *o*-nitrobenzyl ester bond was created. After that, we removed the Boc-protecting group by trifluoroacetic acid to reveal the amine group for reacting with the β-

carboxyl group of folic acid to synthesize the Fa-ONB lipid. The allyl protecting group was removed from the compound by tetrakis (triphenylphosphine) palladium (0) to increase the water solubility of the lipid. Once the *o*-nitrobenzyl ester bond has been formed, the molecules are sensitive to pH and ambient light, so thorough drying of solvents and protection from light are essential for the success of the synthesis. Furthermore, it is important to remove any residual trifluoroacetic acid by repeated column chromatography.

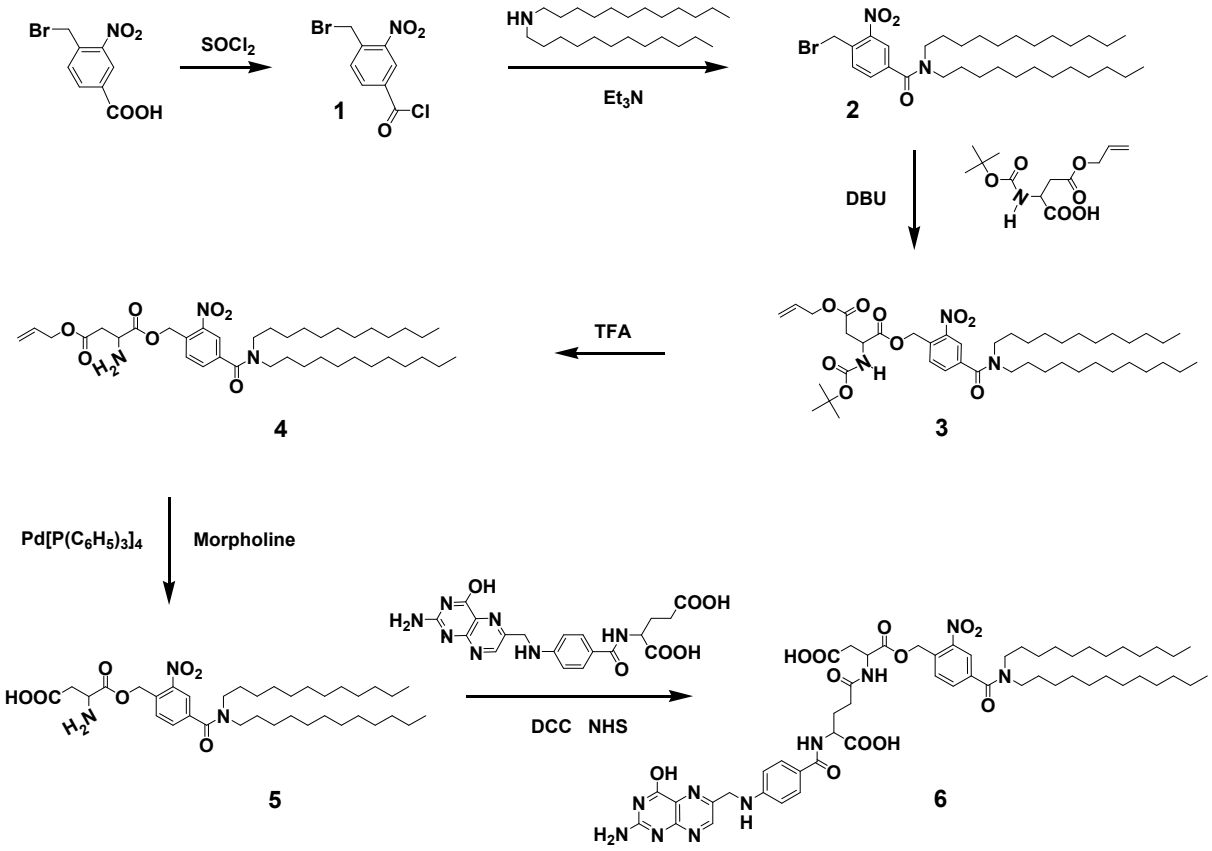

Scheme 2. The synthesis route of the Fa-ONB lipid; Et_3N: triethylamine; DBU: 1,8-Diazabicyclo[5.4.0] undec-7-ene; TFA: trifluoroacetic acid; DCC: Dicyclohexylcarbodiimide; NHS: N-Hydroxysuccinimide;

3.2 The pH-based light-responsiveness of the Fa-ONB lipid

We explored the dissociation effects of pH and UV Fa-ONB lipids at the molecular level, before investigating the release properties of liposomes formed by Fa-ONB lipid. First, the Fa-ONB lipid sealed in a quartz tube was continuously irradiated with different lengths of time (UV light, 365 nm, 60 W). In the UV absorption spectrum (Figure 1c), the peak at 285 nm

decreases significantly, and the intensity of the peak at 378 nm has increases. Moreover, the peak changes are strongest within 0-30 min, which means the photolysis is a rapid process. Samples were collected at 0, 5, 60, 120 min to record the IR spectrum and perform TLC. As shown in Figure S8, after 5 min of illumination, the peaks of $\upsilon_{as}NO_2$ at 1506-1430 cm^{-1} and the peak of υ_sNO_2 at 1430-1330 cm^{-1} largely disappeared, while the stretching vibration peak of Ar-NO appeared at 1310-1214 cm^{-1}. That means there was significant dissociation occurring after only 5 minutes of irradiation as the Ar-NO_2 in the Fa-ONB lipid was converted to Ar-NO. Similarly, TLC (Figure S9) shows that the Fa-ONB lipid disappeared upon illumination while a more hydrophobic (less polar) compound was generated. Mass spectrometry identified one of the cleavage products (Figure S10) by the molecular ion($[M+Na]^+$) at *m/z* 539.4487 as N,N-di-dodecyl-4-formyl-3-nitrosobenzamide (**7**),[47] confirming photolysis of the Fa-ONB lipid by a Norrish type-II reaction as shown in Figure 1a.

Next, we investigated the pH-induced cleavage of Fa-ONB by dissolving the lipid in different phosphate buffers (pH=4.2, 6.5, 7.4, 8.0 and 8.5). TLC (Figure S11 in the Supporting Information) indicated cleavage of Fa-ONB lipid at pH values corresponding to an abnormal physiological environment, and the further the pH value was far away from physiological level (higher or lower), the greater degree of the cracking observed.[68] Samples at pH=6.5 and pH=8.5 were selected for analyzing changes in the IR spectra (Figure S12) and showed that the $\upsilon_{as}NO_2$ and υ_sNO_2 did not disappear after dissociation, i.e., that the Ar-NO_2 moiety still exists after hydrolysis. Mass spectrometry showed (Figure S13) that the Fa-ONB was hydrolyzed at pH=6.5, with a characteristic peak at *m/z* 533.46 $[M+H]^+$ corresponding to *N*,*N*-didodecyl-4-(hydroxylmethyl)-3-nitrobenzamide (**8**; this compound unambiguously identified using MS and NMR (Figures S14, S15) after separation by column chromatography). We thus verified the acid-driven cleavage mechanism of Fa-ONB lipid as shown in Figure 1b. By comparing its solution with saturated NaCl, it was confirmed that the Fa-ONB lipid exhibits excellent pH buffering ability (Figure 1d), which is beneficial to the differential release at the tumor site. In summary, the above results demonstrate that the Fa-ONB lipid is susceptible to cleavage by the two designed inducing stimuli (pH and light).

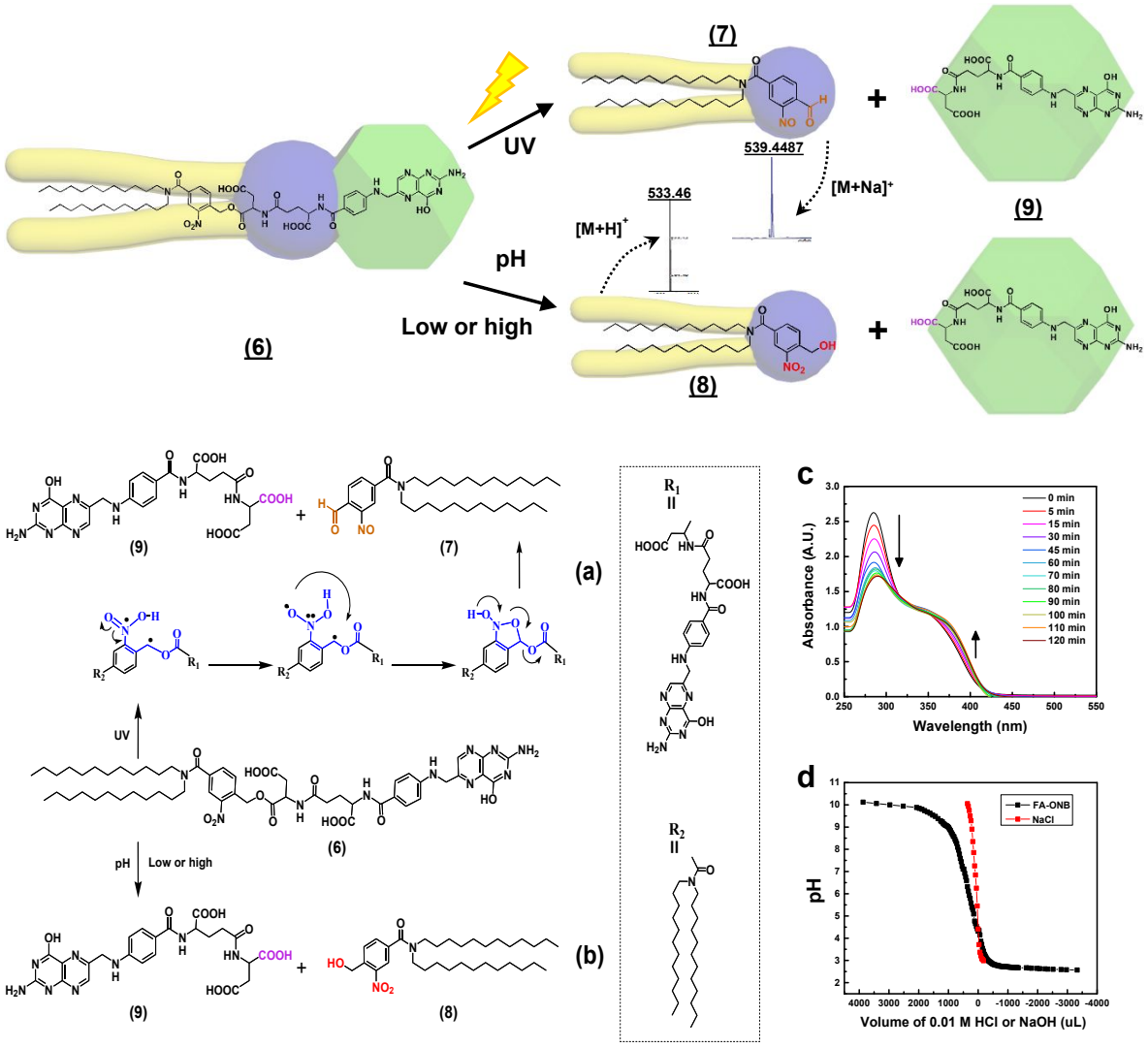

Figure 1. pH and light can cleave the Fa-ONB lipid in two different mechanisms with different lipid fragments. (Top) Mechanism of photolysis (a) and acid-catalyzed hydrolysis (bottom, b) of Fa-ONB. (c) The UV absorption spectrum shows the photolysis of the Fa-ONB lipid. (d) Buffering capacity of the Fa-ONB lipid (with saturated NaCl solution as the control).

3.3 Effect of ultraviolet on the morphology of Fa-ONB liposomes under different pH environments

After confirming that the Fa-ONB lipid is sensitive to pH-triggered hydrolysis and photolysis, we investigated whether this lipid cleavage provides benefits for releasing drugs encapsulated by liposomes. Fa-ONB lipids were compounded with different proportions of the neutral lipid DOPC to select the best performing liposomes for subsequent studies. As shown in Figures S18 and S19 in the Supporting information, Fa-ONB forms liposomes, and zeta potential

measurements of mixed lipid liposomes and mixtures of liposomes demonstrate that the Fa-ONB lipid and DOPC form mixed (FOBD) liposomes. While we prepared liposomes by sonication of hydrated lipid films to compare whether different proportions of DOPC and Fa-ONB lipids would affect the size of FOBD liposomes, FOBD liposomes may also be prepared by extrusion to yield particles of a smaller, composition-independent size (see Figure S20 in the Supporting Information). Four different pH phosphate buffers were selected to model *in vivo* conditions: pH=8.5, as a control condition (slightly alkaline); pH=7.4, physiological environment; pH=6.5, the slightly acidic extracellular environment of the tumor; and pH=4.2, the acidic environment in late endosomes/lysosomes. The induced morphological and dimensional changes were studied by irradiating 0.25 mM empty FOBD73, FOBD55, FOBD37 liposomes different lengths of times in those buffers. In neutral PBS without light illumination, FOBD liposomes are stable for at least 15 days: Figure S16 and Figure S17 show the size and UV absorption of unirradiated FOBD55 liposomes over time; the particle size is maintained around 200 nm, and the UV absorption spectrum does not change.

Figures 2b, 2e and 2h show the changes in the UV absorption spectrum of FOBD55 liposomes during continuous illumination for 120 min in different pH environments. At each pH, the peak intensity at 282 nm decreases and the peak intensity at 340 nm increases with increasing illumination time. Moreover, the lower the pH of the suspension, the greater was the observed variation of peak heights. By comparing with the UV spectral changes of FOBD73 and FOBD37 in Figure 2a, 2d, 2g and Figure 2c, 2f, 2i, it can be inferred that the greater the proportion of Fa-ONB in the FOBD liposome, the more pronounced the curve changes. Figure 2j shows the particle size of the FOBD55 liposome varies with UV exposure time in PBS. In UV irradiation groups, the particle size of the liposomes was initially about 200 nm. Subsequently, the size and width distribution of the liposomes gradually increased with the increase of irradiation time. After 120 min of exposure, the average size of FOBD55 liposomes reached 1000 nm, nearly five-fold.

We also found that there are two peaks in the size distribution determined with DLS in the late stage (60 min and more) of illumination, with the second peak at a size below 100 nm. A

possible explanation for this peak, which is near the size range expected for micelles, is that the folic acid derivative arising from cleavage of the Fa-ONB lipid (compound 9, see Figure 1), which has a hydrophobic core with (hetero)aromatic moieties and several charged groups at the periphery (at neutral pH) self-assembles into micelles (or small, nonmicellar aggregates). Figure 3a compares the change in particle size of illuminated FOBD liposomes (FOBD73, FOBD55, and FOBD37) in buffers of different pH with the control group of DOPC liposomes. With increasing illumination time and greater deviation from pH=7.4, all FOBD liposomes display a growth in size, which indicating that the morphology of liposomes can be gradually adjusted by UV exposure or pH stimulation. In particular, when the pH of the surrounding buffer changed from 7.4 to 4.2, the particle size of the three unirradiated FOBD liposomes increased from ~200 nm to ~400 nm, again indicating that the FOBD liposomes have excellent pH-induced release potential. The pH-dependent change in liposomes with increasing UV exposure time is consistent with the desirable photo-release effect in the acidic environment of the tumor, which can be beneficial to protecting normal tissues during photo-treatment. Interestingly, unlike in the UV absorption spectrum changes, the proportion of Fa-ONB lipids has only a weak effect on the change in particle size, suggesting that the change in liposome structure is slower than the molecular changes.

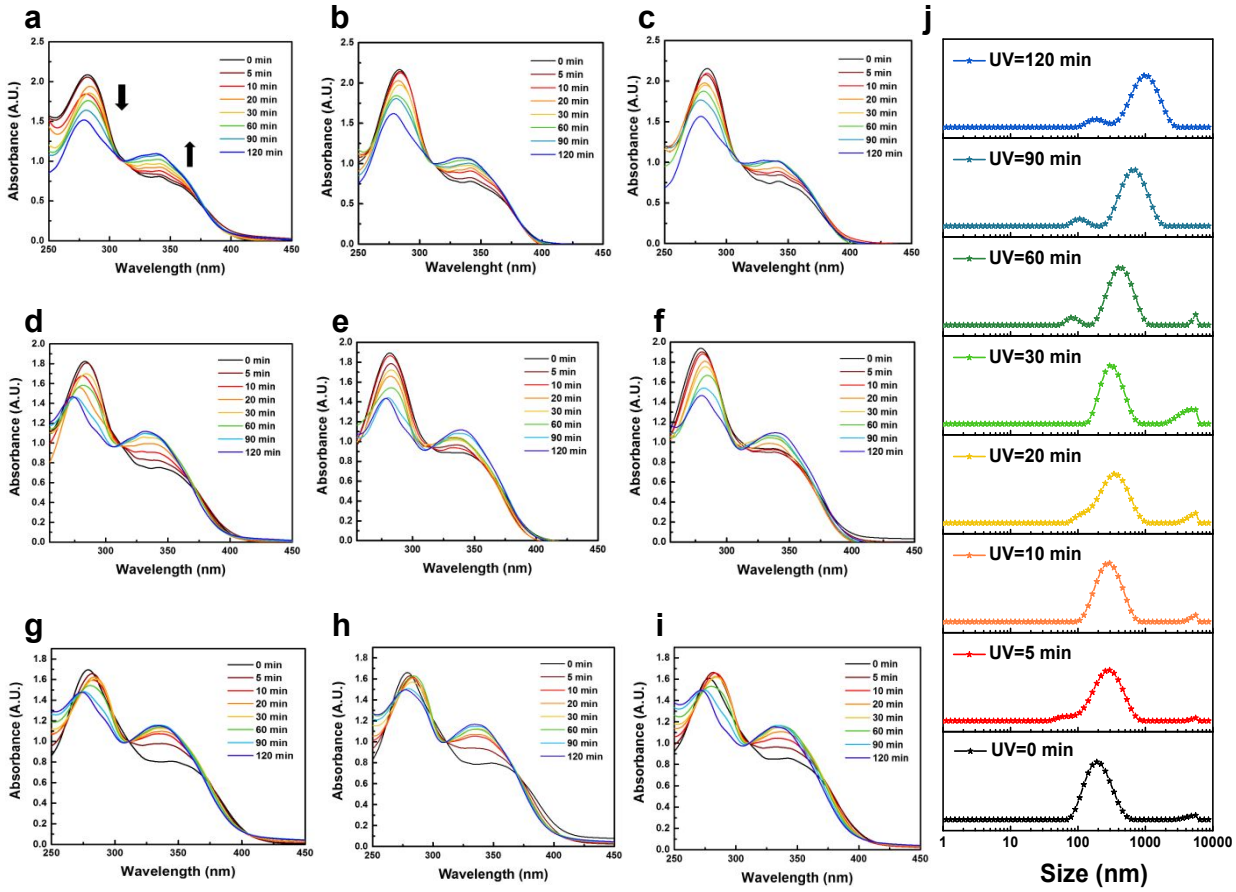

Figure 2. The effect of UV irradiation on FOBD liposome size and morphology at different pH environments. (a-c) The change of the UV absorption spectrum of FOBD73, FOBD55 and FOBD37 liposomes at pH=7.4 (left to right). (d-f) The change of the UV absorption spectrum of FOBD73, FOBD55 and FOBD37 liposomes at pH=6.5 (left to right). (g-i) The change of the UV absorption spectrum of FOBD73, FOBD55 and FOBD37 liposomes at pH=4.2 (left to right). (j) Representative data, the particle size of the FOBD55 liposome varies with UV exposure time.

Transmission electron microscopy (TEM) was used as another method to analyze the cleavage of FOBD liposomes. As shown in Figure 3b and Figure 3d, TEM showed that the unexposed empty FOBD55 liposome was a regular 200 nm double-layered sphere. After 10 minutes of UV exposure, a large number of medium-sized vesicles of about 400 nm began to appear, and the average size of the liposomes increased to about 280 nm (Figure 3c and 3e). After 60 min of illumination, the small vesicles around 200 nm in the solution have almost disappeared, but

larger vesicles around 800 nm have appeared. The average size of nano-particles is now increased to approximately 360 nm (Figure 3f).

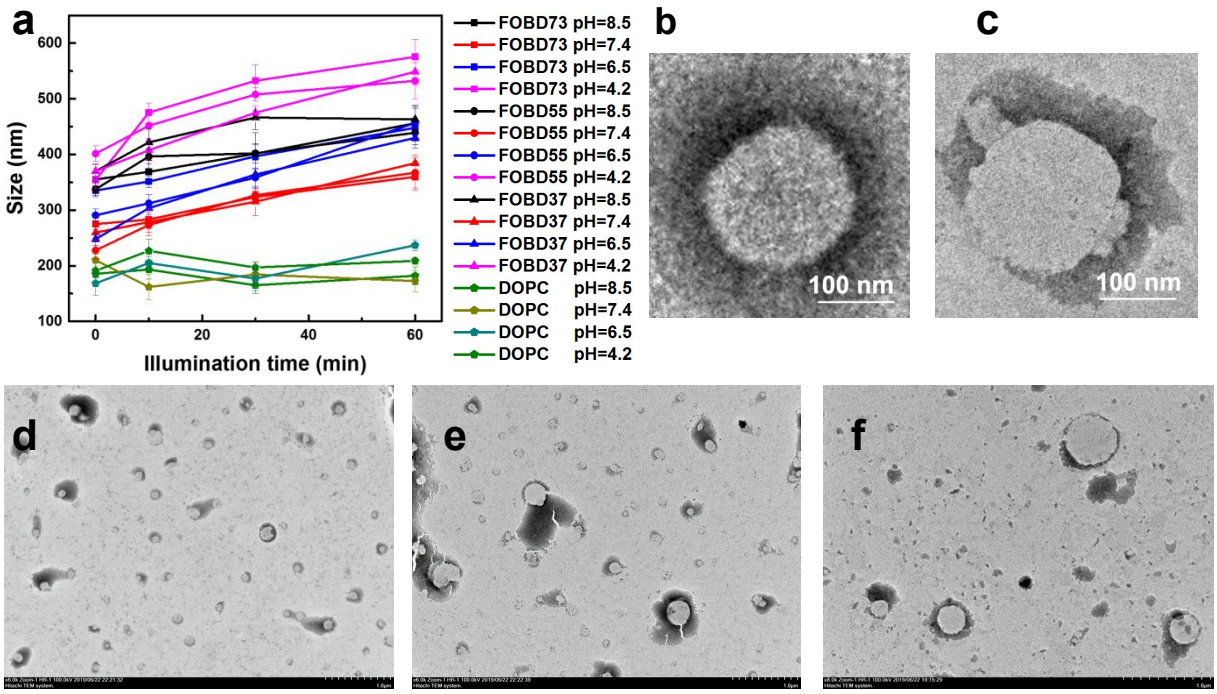

Figure 3. The effect of light treatment on the morphology and size of FOBD liposomes. (a) The size change in empty FOBD liposomes at different pH environment with different lengths of UV exposure time (b) TEM micrograph of one FOBD55 liposome (before UV irradiation). (c) TEM imaging of one cleaving FOBD55 liposome (The Fa-ONB lipids is dissociating and reconstructing to a new liposome, after 10 min of irradiation). (d) A lower-magnification TEM micrograph of FOBD55 liposomes prior to UV irradiation. (e) A lower-magnification TEM micrograph of FOBD55 liposomes after 10 min of UV irradiation (f) A lower-magnification TEM micrograph of FOBD55 liposomes after 60 min of UV irradiation.

3.4. Characterization of Light- and pH-triggered release in DOX/FOBD liposomes

For investigating the triggered release capability of drug-loaded FOBD liposomes, we chose to encapsulate doxorubicin hydrochloride (DOX, a well-studied anticancer drug with self-fluorescent) as a drug-loaded model. Therefore, fluorescence signal can be used for assessing the active targeting ability of DOX-loaded FOBD liposomes (DOX/FOBD liposomes) *in vivo*. Using confocal microscopy, we showed that DOX can be encapsulated in FOBD liposomes (see Figure S21 in the Supporting Information). We then measured the encapsulation efficiency

of FOBD liposomes and DOPC liposomes (Figure 4a). It can be seen that the larger the proportion of FA-ONB lipid in the mixed lipid, the worse the encapsulation efficiency. A similar trend is observed when encapsulation efficiency is measured more qualitatively by the extent of reduction of DOX fluorescence (via self-quenching) that occurs upon encapsulation (Figure S22 in the Supporting Information). As the drug encapsulation rate of FOBD10 liposomes is only 37.52%, it is conceivable that if Fa-ONB lipid is used as a drug carrier alone, it may cause leakage of the drug *in vivo*, which is not conducive to precise treatment. Therefore, only DOPC composite liposomes were used for further studies. The encapsulation efficiency of both FOBD55 and FOBD37 liposomes is greater than 69%, which is higher than most reported drug loading systems[71-73].

The experiments presented in the previous section confirmed that the environmental pH plays a role in accelerating the lysis of FOBD liposomes. For this reason, we prepared the DOX/FOBD liposomes in a PBS environment and exposed them to ultraviolet light for different lengths of time to study the relationship between size and illumination conditions. Figure 4b and 4c show that with increasing exposure time (0–60 min), the size of the nanoparticles progressively increased from 290 nm (see also TEM data, Figure 4d, unlike Doxil[74-78]) to 700 nm with a broadened size distribution. Continually extending the irradiation times, the diameter of the liposomes decreased fast and finally dropped to about 400 nm (see also TEM data; Figure 4e). At the same time, a red (DOX containing) precipitates (Figure 4f) rapidly appear in UV-exposed samples, indicating that, as expected, ultraviolet light is a suitable trigger for accelerating the releasing process of FOBD liposomes. Figure 4b also shows the particle size changes of DOX/FOBD73, DOX/FOBD55 and DOX/FOBD37 under the same conditions. It can be seen from the figure that the change is largest for DOX/FOBD55 liposomes, followed by DOX/FOBD73 and finally DOX/FOBD37 liposomes. This is inconsistent with the FOBD data without the drug. We speculate that DOX may electrostatically combine with the fragmented folic acid derivative to form the observed precipitate (Figure 4f) which contains DOX (red color) but is amorphous (see Figure S23, the WAXRD data in Supporting Information). In FOBD73, because of the high content of FA-ONB lipid, the inflection point (after which the particle size of the liposomes begins to decrease)

occurs first (after 40 min of illumination). FOBD55 shows the inflection point after 60 minutes while in FOBD37, because the content of Fa-ONB is small, the change in the particle size is not as obvious as the other two groups. As we have hypothesized before,[54] we speculated that there are two competing behaviors in the dissociation process of DOX/FOBD liposomes. First is the growing phenomenon of liposomes following the cleavage of Fa-ONB lipids, like the dissociation of empty FOBD liposomes. At the beginning (0-60 min), as the resulting ONB lipids are still contained in the cleavage liposomes, the size of liposomes gradually grows, accompanied by an initial release of DOX. Over a longer period of irradiation time (> 60 minutes), the released DOX competitively contains ONB lipids, compound 9, or DOPC to form a precipitate, which results in a reduction in liposome size becomes to the dominant process.

For quantifying the relationship between environmental pH, irradiation time, and release ability, DOX/FOBD liposomes that had been irradiated for different lengths of time, were dialyzed in different buffers. Figures 4g, 4h, and 4i plot the cumulative DOX release curve in four buffers (pH=8.5, 7.4, 6.5 and 4.2) for the irradiated DOX/FOBD73, DOX/FOBD55, and DOX/FOBD37 liposomes, respectively. Note that even the release of free DOX (as measured by the dialysis method) does not reach 100% and is pH-dependent. For all the unexposed samples, an increase in environmental acidity increases not only the cumulative release of DOX, but also the speed of drug release (the slope at 0–6 h). In all four buffer solutions, the release amount and release efficiency of all samples decreased continuously with the UV exposure time of the samples. This counterintuitive effect occurs because the light accelerates the dissociation of the Fa-ONB lipid, especially in a more acidic environment (consider, e.g. DOX/FOBD73 at pH=4.2, comparing the unexposed sample with the sample irradiated for 10 min: release is significantly lower with UV irradiation). The longer the exposure time, the more insoluble doxorubicin precipitate is produced, and the less drug passes through the dialysis membrane. The differences in DOX/FOBD liposome photodissociation and release at different pH can be used to distinguish tumor tissues from normal cells, which can provide further precision in targeted treatment.

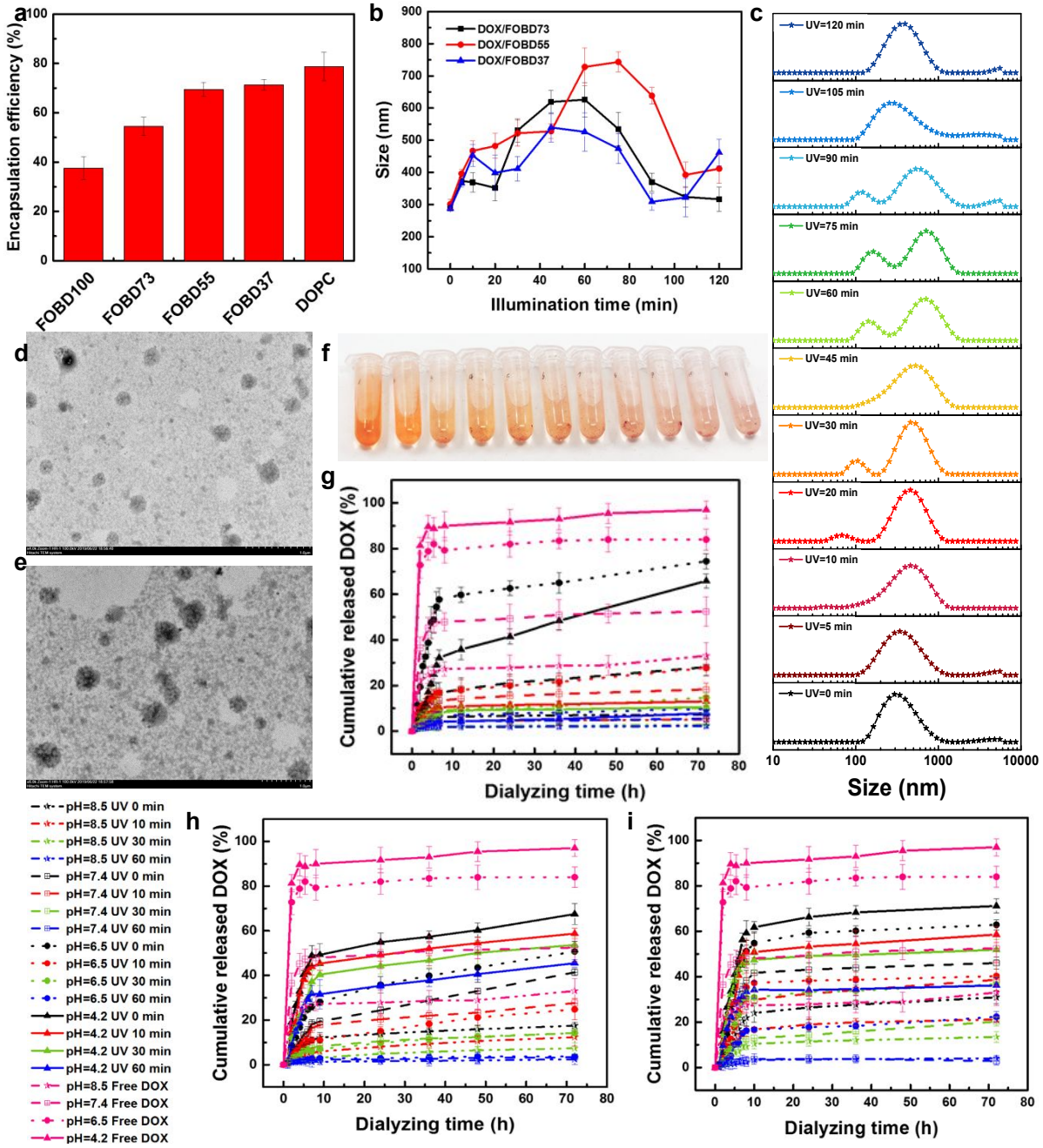

Figure 4. pH- and Photo release properties of DOX/FOBD liposomes *in vitro*. (a) Encapsulation efficiency of DOX/FOBD liposomes compared with DOPC liposomes. (b) The relationship between particle size change and exposure time of DOX/FOBD73, DOX/FOBD55 and DOX/FOBD37 in PBS. (c) The changes in the size of DOX/FOBD55 liposomes with different UV exposure time (in PBS). (d) A TEM micrograph of an unexposed DOX/FOBD55 liposome sample. (e) TEM imaging of the supernatant of the exposed DOX/FOBD55 sample (120 min). See Figure S24 in the Supporting Information for the original (full-size) TEM micrographs. (f) Macroscopic appearance of exposed DOX/FOBD55 liposomes (the time

interval is the same as in Figure 4c). The DOX-containing (red) precipitate is formed and increased with the irradiation time. (g) The cumulative release of DOX from FOBD73 liposomes at different lengths of UV exposure time (UV light, 0, 10, 30, and 60 min) in four pH environments. (h) Cumulative release curve of FOBD55 liposomes, same conditions as (g). (i) Cumulative release curve of FOBD37 liposomes, same conditions as (g).

3.5. Performance of FOBD liposomes in cells

3.5.1 Cytotoxicity of FOBD and DOX/FOBD liposomes

Macrophages (Raw 264.7), breast cancer cells (MCF-7), cervical cancer cells (Hela7702) and liver cancer cells (HepG2) were used to assess the targeting and cytotoxicity of FOBD and DOX/FOBD liposomes. As shown in Figures 5a-c and Figure S25 (cytotoxicity of empty DOPC liposomes), the higher the concentration of FOBD, the greater the toxicity to these four cells. An increase of Fa-ONB lipid content in FOBD liposomes did not change the toxicity to macrophages, liver cancer, and breast cancer cells but significantly increased cytotoxicity against Hela cells, which suggests that the Fa-ONB lipid has a stronger targeting effect on Hela cells. For the subsequent studies of the targeting effect of FOBD liposomes and their ability to target cancer cells over normal cells, we selected 0.25 mM as the concentration of FOBD liposomes to encapsulate DOX and test the cytotoxicity of the drug-loaded liposomes.

To study the light-triggered delivery of DOX by FOBD liposomes, we first irradiated the four selected types of cells with UV light for 0-20 min (365 nm, 60 W) to determine the damage to cells from exposure to UV light. As shown in Figure 5d, the viability of cells only decreased slightly. We then added 0.25 mM DOX/FOBD liposomes (same amount of loaded DOX in all samples) to cells and exposed them under ultraviolet light for 0, 10 or 20 minutes. After 24 hours, the survival of Hela cells in the DOX-loaded FOBD group was significantly reduced compared to the DOX/DOPC and free DOX groups, and the higher the content of Fa-ONB in the mixed liposomes, the lower the survival of the Hela cells. For the light-treated group, the viability of all four cell lines gradually decreased with increasing irradiation time. This shows that the drug release as measured by dialysis is not necessarily indicative of release inside cells (i.e., the precipitate remains biologically active or formation of the precipitate is suppressed

inside the cell) and suggests that additional phototherapy can precisely regulate the release of DOX.

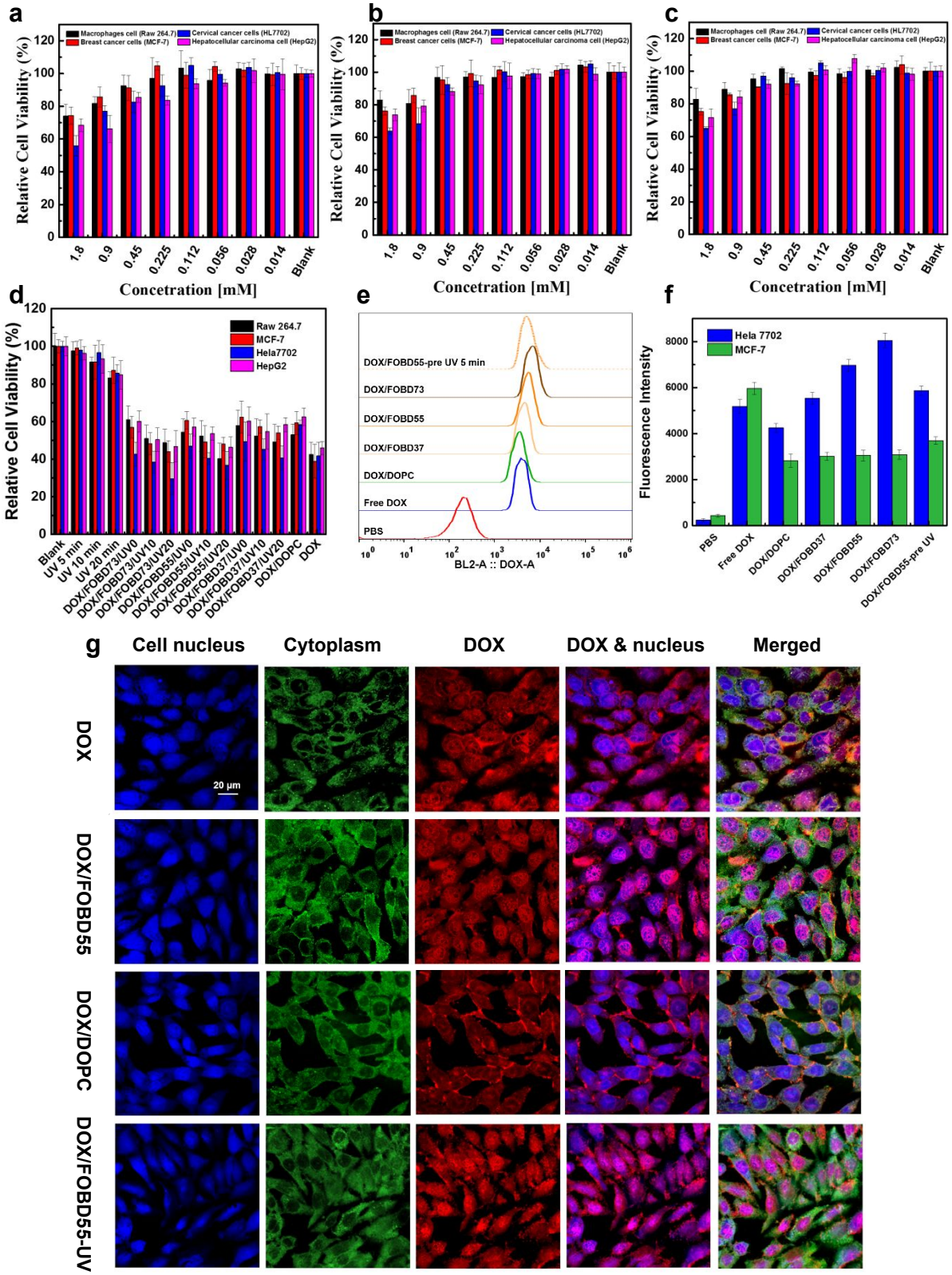

Figure 5. The cytotoxicity of FOBD and DOX/FOBD liposomes. (a) Cytotoxicity of FOBD73 liposomes versus concentration, against (Raw 264.7, MCF-7, Hela7702, and HepG2). (b) Cytotoxicity of FOBD55 liposomes. (c) Cytotoxicity of FOBD37 liposomes. (d) The effect of active targeting and UV treatment, free DOX, 0.25 mM DOX/FOBD liposomes and 0.25 mM DOX/DOPC liposomes on the viability of Raw 264.7, MCF-7, Hela7702 and HepG2 cells. (e) Flow cytometry of DOX in HeLa cells after 90 min incubation with DOX, DOX/DOPC, DOX/FOBD73, DOX/FOBD55, DOX/FOBD37 and pre-exposed DOX/FOBD55 liposomes. (f) The uptake of DOX in free DOX, DOX/DOPC, DOX/FOBD73, DOX/FOBD55, DOX/FOBD37 and pre-exposed DOX/FOBD55 groups were compared between HeLa and MCF-7 cells (flow cytometry data, BL2-A DOX). (g) Confocal imaging of free DOX, DOX/DOPC, DOX/FOBD55 and pre-exposed DOX/FOBD55 liposomes on Hela cells after 90 min of incubation.

3.5.2 Cellular uptake of DOX/FOBD liposomes

Flow cytometry was used to test the uptake of FOBD liposomes and control samples in HeLa cells. As shown in Figure 5e, DOX/DOPC has the lowest uptake rate, followed by free DOX. This difference likely stems from the fact that free small DOX molecular can enter the cells by diffusion, but for the larger liposomes, they entry into cells depends on the slower process of endocytosis. It is worth noting that the FOBD groups had the highest uptake rate which also gradually increased with the increase in the proportion of Fa-ONB lipid in the mixed liposome. This is likely because Fa-ONB lipids can target folate receptors on Hela cells and thus enter cells most rapidly via active transport mechanisms. Although FOBD73 liposomes showed the best targeting ability, their drug encapsulation ability is weak and could lead to drug leakage *in vivo*. Therefore, DOX/FOBD55 liposomes were selected for further testing.

We next studied the photo-dissociation properties of DOX/FOBD55 liposomes inside of cells. After 2.5 hours, the above-mentioned DOX-loaded liposome group was almost saturated in the uptake of the living cells. In addition, flow cytometry only yields the fluorescence intensity of whole cells, meaning that it is unable to distinguish whether DOX is in the cytoplasm or the nucleus. Therefore, we prepared another sample that was dissociated by UV irradiation before

adding it to the cells, to use the differential intake of free DOX and DOX/FOBD to test its photolysis characteristics. In Figure 5e, the cellular uptake of the UV pre-treated DOX/FOBD55 liposome group was between the DOX/FOBD55 group and the free DOX group, again validating our hypothesis that FOBD liposomes can be partially dissociated after a short time illumination, releasing a small amount of free DOX. A reduction in intact Fa-ONB lipids in this sample by the photolysis results in a reduced targeting effect and a decrease in cellular uptake.

We used flow cytometry with cells expressing (HeLa) and not expressing (MCF-7) folate receptors to further verify the targeting and photolysis properties of DOX/FOBD liposomes.[79, 80] As shown in Figure 5f, the increasing proportion of Fa-ONB lipid in the mixed liposomes had no significant effect on the uptake by MCF-7 cells but led to an increase in uptake by HeLa cells, demonstrating the selective targeting ability of FOBD liposomes. In the MCF-7 cells, the cellular uptake of DOX for the pre-UV group was higher than that of any of the FOBD groups. This is because, for the MCF-7 group, both the DOX/DOPC and DOX/FOBD groups slowly entered the cells by endocytosis (rather than receptor-mediated endocytosis as in the HeLa cells), whereas the free DOX transferred into the cells at a faster rate. In the pre-UV group, part of the FOBD liposomes dissociated due to the exposure to light, releasing free DOX and accelerating the rate of DOX entering the cell.

For a visual comparison of their effects, free DOX, DOX/DOPC, DOX/FOBD55, and pre-treated DOX/FOBD55 liposomes were applied to Hela cells and the cells incubated for 90 min before imaging by confocal microscopy (Figure 5g). Consistent with the data in Figure 5e, the fluorescence of DOX was evenly distributed in the nucleus and cytoplasm in cells treated with free DOX. However, in cells treated with DOX/DOPC, the fluorescence of DOX was mainly in the cytoplasm. DOX/FOBD55 liposomes enter the cells faster, and the DOX carried by them is mainly enriched in the nucleus. In the pre-illuminated DOX/FOBD55 group, since the FOBD55 liposomes were partially lysed and released some of the free DOX prior to application to the cells, DOX was observed in both the cytoplasm and nucleus (with the fluorescence in the nucleus less than that in the DOX/FOBD55 group). The above data again confirmed that

FOBD liposomes have active targeting ability and photo-release capabilities which can be fine-tuned by UV irradiation.

3.6. The tumor targeting and dual triggering performance of DOX/FOBD liposomes *in vivo*

The real-time fluorescence imaging system was used for further investigating the active targeting and dual-trigger release capabilities of DOX/FOBD55 liposomes *in vivo*. The detection of DOX fluorescence can be used to determine the location of FOBD liposomes, as Fa-ONB and DOPC are nonfluorescent. To assess for active targeting ability, we chose DOX/DOPC liposomes as the control group. As shown in Figure 6, at 0.5 h post-injection, both DOX/DOPC and DOX/FOBD liposomes were visible at the tumor site. However, after 1 h of injection, the brighter fluorescence of the tumor site in the DOX/FOBD55 group indicates that the FOBD liposomes aggregate more rapidly in tumors than the DOPC liposomes that have only EPR capabilities (passive targeting). At 2 h post-injection, the fluorescence intensity at the tumor site is almost equivalent, suggesting that most of the liposomes (both DOX/DOPC or DOX/FOBD) have accumulated at the tumor site. At this time, the tumor site of the phototherapy group was intermittently irradiated with UV light to accelerate the uptake of DOX by the nucleus. At 4 h post-injection, the fluorescence intensity of the DOX/DOPC group began to decrease, while the DOX/FOBD groups (with and without photo-treatment) were almost unchanged (showing even a slight increase). We speculate that at this time, a large quantity of DOX/DOPC vesicles at the tumor site are cleared by metabolism while in the DOX/FOBD and DOX/FOBD-UV groups, due to their active targeting ability and subsequent cellular uptake, the fluorescence intensity remains high. At 6 h and 12 h post-injection, although the fluorescence intensity of the DOX/FOBD groups (with and without photo-treatment) is gradually weakened, it remains significantly higher than the DOX/DOPC group, confirming the active targeting of FOBD liposomes. In addition, *ex vivo* imaging of organs and excised tumors shows both DOX/FOBD liposome groups produced a stronger DOX signals at the tumor site than that in DOX/DOPC group, especially for the DOX/FOBD with light treatment group.

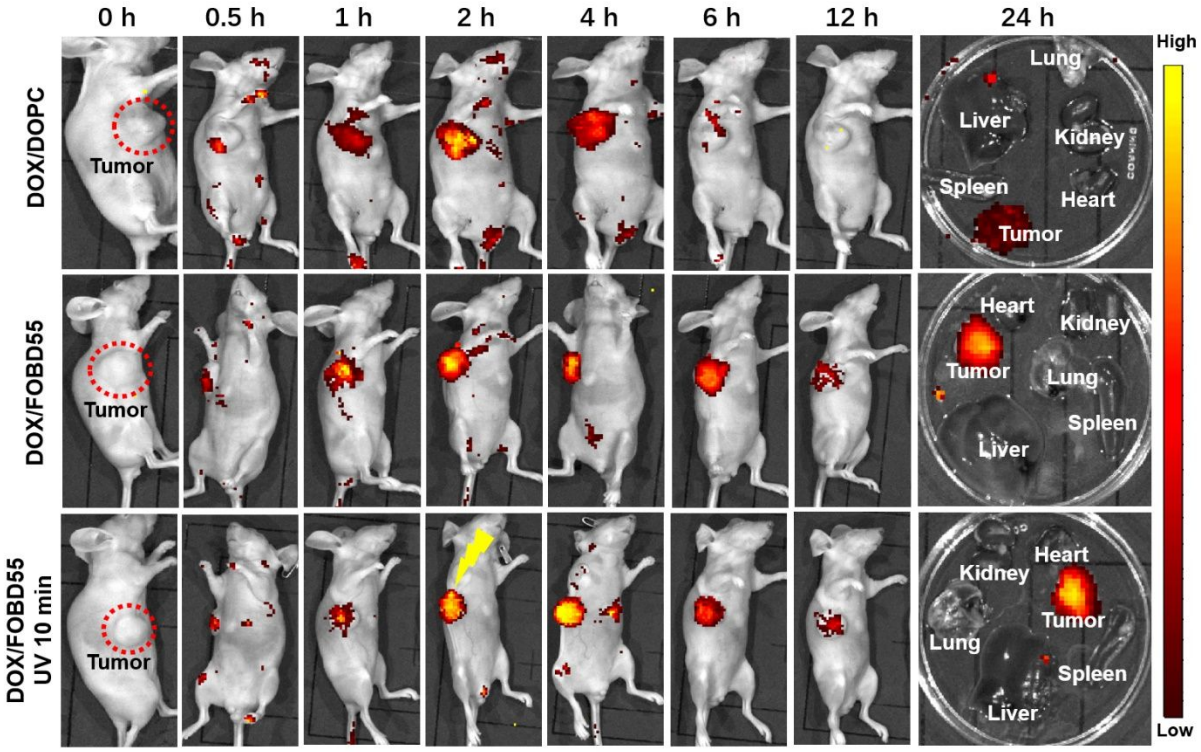

Figure 6. *In vivo* fluorescence imaging of mice with different treatment regimens

3.7. Tumor suppression study

HeLa tumors were implanted under the armpit of nude mice to evaluate the chemotherapy effect of DOX/FOBD liposomes. The mice were randomly divided into 5 groups: control (PBS), free DOX, DOX/DOPC, DOX/FOBD55 and DOX/FOBD55-UV. Tumors were treated over 30 days (Every 2 days, injection 200 μL; DOX dose 2.5 mg/kg; the tumor site in the light-treatment group were intermittently exposed to ultraviolet light (365 nm, 60 W) for 10 min, after 2 h of injection). As shown in Figure 7a and 7b, within 30 days, in the PBS (control) group, the tumor volume increased rapidly from 95 to 1815 mm^3 (while the body weight increased from 19.19 to 23.49 g). In the free DOX group, the treatment inhibited the growth of tumors (99 to 691 mm^3), but showed strong side effects (body weight from 19.15 to 16.22 g). Compared to the DOX/DOPC group (96 to 479 mm^3, 19.42 to 22.56 g), the tumor treatment was more successful in the DOX/FOBD55 group (95 to 316 mm^3, 19.53 to 22.80 g). A possible explanation for this therapeutic effect is the active targeting and acidic (tumor environment) cleavage of FOBD liposomes. The DOX/FOBD-UV group displayed the most obvious tumor inhibition effect (95 to 239 mm^3, body weight from 20.28 to 22.94 g), once again confirming

that photo-release can effectively enhance the release of DOX and promote cancer cell apoptosis. Figures 7c shows the resected tumors after the end of treatment protocol for more direct observation of the treatment efficacy in each group. After sectioning and H&E staining, confocal microscopy (Figure 7d and 7e) was used to reveal the uptake of DOX in each tumor section (observing DOX intensity signal (green fluorescence)). As can be seen, the fluorescence of DOX in the light-therapy group is highest, the DOX/FOBD group is second-highest, the DOX/DOPC group is the third and the free DOX group is lowest, which is accordant with the resected tumor fluorescence imaging data in Figure 6. This again confirms that light therapy can further improve the release efficiency of FOBD liposomes. In Figure 7f, H&E staining of the organs and tumor of the mice were used for histological evaluating the biocompatibility of DOX/FOBD in the DOX/FOBD and DOX/FOBD-UV groups. Unlike the unclear membranes and inflammatory infiltration of the liver section observed for the free DOX group, all other major organ sections in the PBS, DOX/DOPC, DOX/FOBD, DOX/FOBD-UV groups showed negligible damage. Therefore, the results of therapeutic and histological analyses prove the prospect of multifunctional FOBD liposomes in low toxicity treatment applications.

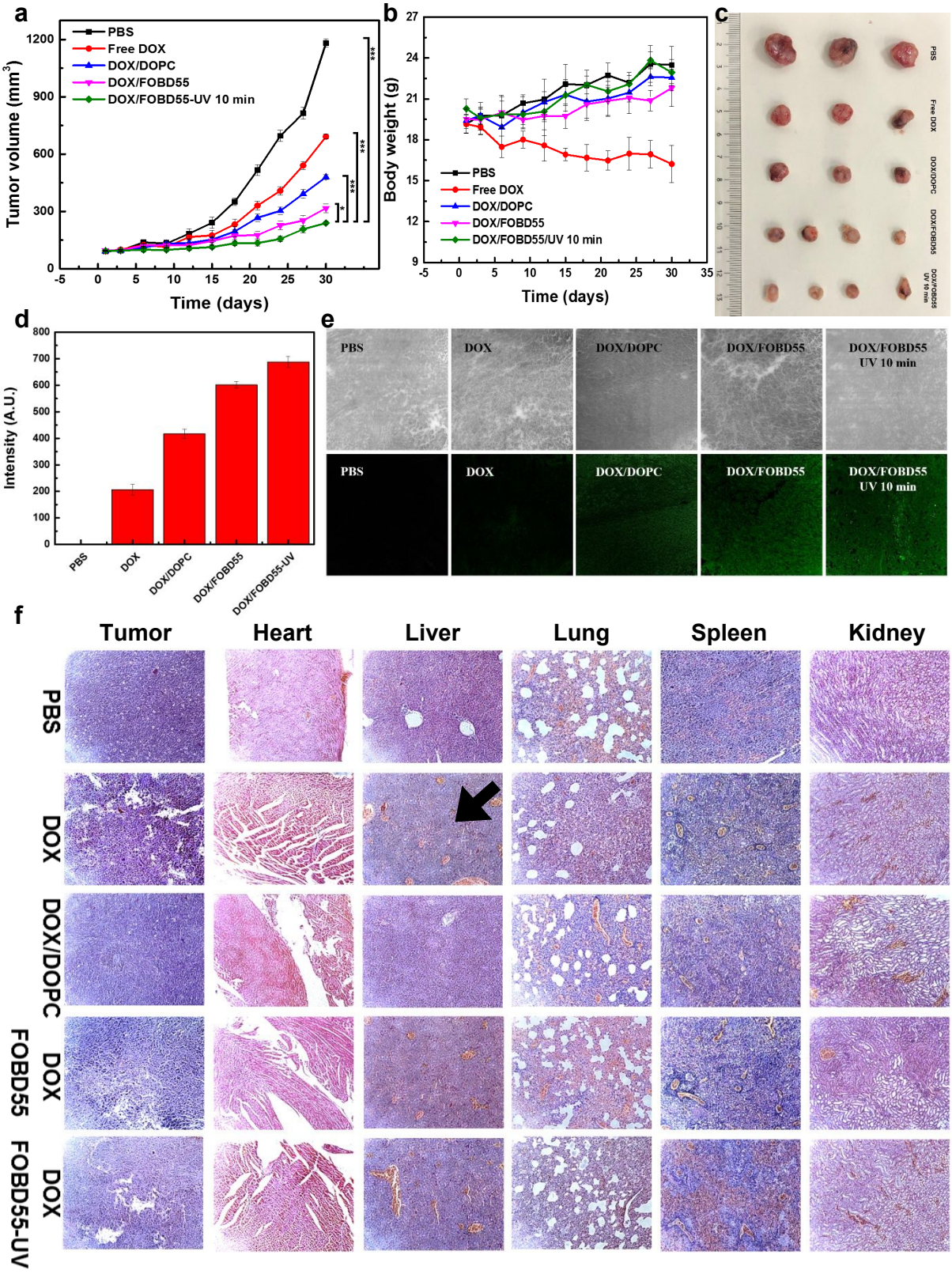

Figure 7. The tumor suppression study of DOX/FOBD55 liposomes. (a) The average cervical tumor volume varies with treatment time (*: $p < 0.09$, ***: $p < 0.001$; $p = 0.082796$ for DOX/FOBD55 to DOX/FOBD55-UV group). (b) The average body weight of mice varies with treatment time. (c) Excised

tumor of mice (day 30, end of the therapeutic protocol). (d) Comparison of the average fluorescence intensity of tumor sections (e) Confocal fluorescence (Olympus FV1000, 20×) slice imaging of tumor tissue in different treatment protocols. The top is the brightfield images and the bottom shows the fluorescence (DOX) channel images (green). (f) Representative micrographs (20×) of stained (hematoxylin and eosin) slices from tumor and main organs. Black arrow indicates the unconventional morphology of mouse liver cells.

4. Conclusion

We designed and synthesized a new lipid (Fa-ONB) for self-assembly into a drug carrier with the ability to actively target the tumor tissue and a dual-source response to modulate drug release for precise medical treatment. DOX/FOBD liposomes showed a pH-triggered release ability and the release efficiency increased as the difference between environmental pH and neutral pH increased. Exposure to UV light can further trigger liposome lysis and promote the local release of the drug. We demonstrated the active targeting and pH-light dual-induced dissociation properties of FOBD liposomes by flow cytometry, confocal imaging and real-time fluorescence of mouse tumor models. In a xenograft cancer model, both UV-irradiated DOX/FOBD liposomes and DOX/FOBD liposomes inhibited tumor growth more than the DOX/DOPC and free DOX control groups. Ultraviolet radiation improved the treatment efficiency, showing the advantages of synergistic controlled release of light and pH. The proposed work provides a new insight for the design of the precision drug delivery multifunctional liposomes with active targeting and controlled release properties.

5. Acknowledgments

The research was supported by China Scholarship Council Talent International Cooperation Project [2019]13044, International Science & Technology Cooperation Program of China No.2015DFA41670 and the Fundamental Research Funds for the Central Universities DUT19GJ203. Thanks to Chemical Analysis and Research Center for fluorescence imaging at Dalian University of Technology, and the Materials Research Laboratory at University of California Santa Barbara for its support.

Associated content

Supporting Information

Detailed synthesis procedures, additional spectrums of Fa-ONB dissociation properties, stability of FOBD liposomes, method for preparing smaller size liposomes, confocal imaging and full-size TEM figures of DOX/FOBD liposomes, WAXRD spectrum of DOX precipitate, cytotoxicity of empty DOPC liposomes

References

1. Harris, R. E., *Epidemiology of chronic disease: global perspectives*. Jones & Bartlett Learning: **2019**.
2. Nurgali, K.; Jagoe, R. T.; Abalo, R. Adverse effects of cancer chemotherapy: Anything new to improve tolerance and reduce sequelae? *Front. Pharmacol.* **2018**, 9, 245.
3. Pillai, G. Nanotechnology Toward Treating Cancer: A Comprehensive Review. In *Applications of Targeted Nano Drugs and Delivery Systems*; Elsevier: **2019**, pp 221-256.
4. Patra, J. K.; Das, G.; Fraceto, L. F.; Campos, E. V. R.; del Pilar Rodriguez-Torres, M.; Acosta-Torres, L. S.; Diaz-Torres, L. A.; Grillo, R.; Swamy, M. K.; Sharma, S. Nano based drug delivery systems: Recent developments and future prospects. *J. Nanobiotecg.* **2018**, 16, 71-104.
5. Peer, D.; Karp, J. M.; Hong, S.; Farokhzad, O. C.; Margalit, R.; Langer, R. Nanocarriers as an emerging platform for cancer therapy. *Nature Nanotech.* **2007**, 2, 751.
6. Davis, M. E.; Chen, Z.; Shin, D. M. Nanoparticle therapeutics: an emerging treatment modality for cancer. In *Nanoscience And Technology: A Collection of Reviews from Nature Journals*; World Scientific: **2010**, pp 239-250.
7. Petros, R. A.; DeSimone, J. M. Strategies in the design of nanoparticles for therapeutic applications. *Nat. Rev. Drug Discov.* **2010**, 9, 615.
8. Rosenblum, D.; Joshi, N.; Tao, W.; Karp, J. M.; Peer, D. Progress and challenges towards targeted delivery of cancer therapeutics. *Nat. Commun.* **2018**, 9, 1410.
9. Danhier, F.; Feron, O.; Préat, V. To exploit the tumor microenvironment: passive and active tumor targeting of nanocarriers for anti-cancer drug delivery. *J. Controlled Release.* **2010**, 148, 135-146.
10. Hirsjarvi, S.; Passirani, C.; Benoit, J.-P. Passive and active tumour targeting with nanocarriers. *Curr. Drug Discov. Technol.* **2011**, 8, 188-196.
11. Bertrand, N.; Wu, J.; Xu, X.; Kamaly, N.; Farokhzad, O. C. Cancer nanotechnology: the impact of passive and active targeting in the era of modern cancer biology. *Adv. Drug Delivery Rev.* **2014**, 66, 2-25.
12. Gu, F. X.; Karnik, R.; Wang, A. Z.; Alexis, F.; Levy-Nissenbaum, E.; Hong, S.; Langer, R. S.; Farokhzad, O. C. Targeted nanoparticles for cancer therapy. *Nano today.* **2007**, 2, 14-21.
13. Llovet, J. M.; Bruix, J. Molecular targeted therapies in hepatocellular carcinoma. *Hepatology.* **2008**, 48, 1312-1327.
14. Tsuruo, T.; Naito, M.; Tomida, A.; Fujita, N.; Mashima, T.; Sakamoto, H.; Haga, N. Molecular targeting therapy of cancer: drug resistance, apoptosis and survival signal. *Cancer Sci.* **2003**, 94, 15-21.

15. Sudimack, J.; Lee, R. J. Targeted drug delivery via the folate receptor. *Adv. Drug Delivery Rev.* **2000**, 41, 147-162.
16. Lu, Y.; Low, P. S. Folate-mediated delivery of macromolecular anticancer therapeutic agents. *Adv. Drug Delivery Rev.* **2012**, 64, 342-352.
17. Leamon, C. P.; Low, P. S. Folate-mediated targeting: from diagnostics to drug and gene delivery. *Drug Discovery Today.* **2001**, 6, 44-51.
18. Zhao, S.; Sun, S.; Jiang, K.; Wang, Y.; Liu, Y.; Wu, S.; Li, Z.; Shu, Q.; Lin, H. In Situ Synthesis of Fluorescent Mesoporous Silica–Carbon Dot Nanohybrids Featuring Folate Receptor-Overexpressing Cancer Cell Targeting and Drug Delivery. *Nano-Micro Letters.* **2019**, 11, 32. doi:10.1007/s40820-019-0263-3
19. Meng, F.; Wang, J.; Ping, Q.; Yeo, Y. Camouflaging Nanoparticles for Ratiometric Delivery of Therapeutic Combinations. *Nano Lett.* **2019**, 19, 1479-1487.
20. Liu, Y.; Dai, Z.; Wang, J.; Tu, Y.; Zhu, L. Folate-targeted pH-sensitive bortezomib conjugates for cancer treatment. *Chem. Commun.* **2019**, 55, 4254-4257.
21. Duthie, S. J. Folic acid deficiency and cancer: mechanisms of DNA instability. *British medical bulletin.* **1999**, 55,578-592.
22. Antony, A. C. Folate receptors. *Annu. Rev. Nutr.* **1996**, 16, 501-521.
23. Parker, N.; Turk, M. J.; Westrick, E.; Lewis, J. D.; Low, P. S.; Leamon, C. P. Folate receptor expression in carcinomas and normal tissues determined by a quantitative radioligand binding assay. *Anal. Biochem.* **2005**, 338, 284-293.
24. Zwicke, G. L.; Ali Mansoori, G.; Jeffery, C. J. Utilizing the folate receptor for active targeting of cancer nanotherapeutics. *Nano reviews.* **2012**, 3, 18496.
25. Gascoigne, K. E.; Taylor, S. S. How do anti-mitotic drugs kill cancer cells. *J. Cell Sci.* **2009**, 122, 2579-2585.
26. Yang, F.; Teves, S. S.; Kemp, C. J.; Henikoff, S. Doxorubicin, DNA torsion, and chromatin dynamics. *BBA-Rev. cancer.* **2014**, 1845, 84-89.
27. Souhami, R.; Tobias, J. S., *Cancer and its management*. John Wiley & Sons: **2008**.
28. Skeel, R. T.; Khleif, S. N., *Handbook of cancer chemotherapy*. Lippincott Williams & Wilkins: **2011**.
29. Zhao, X.; Wei, Z.; Zhao, Z.; Miao, Y.; Qiu, Y.; Yang, W.; Jia, X.; Liu, Z.; Hou, H. Design and development of graphene oxide nanoparticle/chitosan hybrids showing pH-sensitive surface charge-reversible ability for efficient intracellular doxorubicin delivery. *ACS Appl. Mat. Interfaces.* **2018**, 10, 6608-6617.
30. Balamuralidhara, V.; Pramodkumar, T.; Srujana, N.; Venkatesh, M.; Gupta, N. V.; Krishna, K.; Gangadharappa, H. pH sensitive drug delivery systems: A review. *Am J Drug Discov Dev.* **2011**, 1, 24-48.
31. Nahire, R.; Hossain, R.; Patel, R.; Paul, S.; Meghnani, V.; Ambre, A. H.; Gange, K. N.; Katti, K. S.; Leclerc, E.; Srivastava, D. pH-triggered echogenicity and contents release from liposomes. *Mol. pharm.* **2014**, 11, 4059-4068.
32. Sudimack, J. J.; Guo, W.; Tjarks, W.; Lee, R. J. A novel pH-sensitive liposome formulation containing oleyl alcohol. *BBA-Biomembranes.* **2002**, 1564, 31-37.
33. Lee, Y.; Thompson, D. Stimuli ‐ responsive liposomes for drug delivery. *Wiley Interdisciplinary Reviews: Nanomedicine and Nanobiotechnology.* **2017**, 9, e1450.
34. Zhang, D.; Wu, M.; Cai, Z.; Liao, N.; Ke, K.; Liu, H.; Li, M.; Liu, G.; Yang, H.; Liu, X.

Chemotherapeutic Drug Based Metal–Organic Particles for Microvesicle ‐ Mediated Deep Penetration and Programmable pH/NIR/Hypoxia Activated Cancer Photochemotherapy. *Adv. Sci.* **2018**, 5, 1700648.

35. Moorthy, M. S.; Kim, H.-B.; Bae, J.-H.; Kim, S.-H.; Ha, C.-S. Design of core–shell magnetic mesoporous silica hybrids for pH and UV light stimuli-responsive cargo release. *Rsc Adv.* **2016**, 6, 29106-29115.

36. Puri, A. Phototriggerable liposomes: current research and future perspectives. *Pharmaceutics.* **2014**, 6, 1-25.

37. Singh, P.; Choudhury, S.; Kulanthaivel, S.; Bagchi, D.; Banerjee, I.; Ahmed, S. A.; Pal, S. K. Photo-triggered destabilization of nanoscopic vehicles by dihydroindolizine for enhanced anticancer drug delivery in cervical carcinoma. *Colloids Sur.f B Biointerfaces.* **2018**, 162, 202-211.

38. Li, H.; Yang, X.; Zhou, Z.; Wang, K.; Li, C.; Qiao, H.; Oupicky, D.; Sun, M. Near-infrared light-triggered drug release from a multiple lipid carrier complex using an all-in-one strategy. *J. Controlled Release.* **2017**, 261, 126-137.

39. Marturano, V.; Cerruti, P.; Carfagna, C.; Giamberini, M.; Tylkowski, B.; Ambrogi, V. Photo-responsive polymer nanocapsules. *Polymer.* **2015**, 70, 222-230.

40. Zangabad, P. S.; Mirkiani, S.; Shahsavari, S.; Masoudi, B.; Masroor, M.; Hamed, H.; Jafari, Z.; Taghipour, Y. D.; Hashemi, H.; Karimi, M. Stimulus-responsive liposomes as smart nanoplatforms for drug delivery applications. *Nanotechnol. Rev.* **2018**, 7, 95-122.

41. Zhao, H.; Sterner, E. S.; Coughlin, E. B.; Theato, P. o-Nitrobenzyl alcohol derivatives: Opportunities in polymer and materials science. *Macromolecules.* **2012**, 45, 1723-1736.

42. Fomina, N.; McFearin, C.; Sermsakdi, M.; Edigin, O.; Almutairi, A. UV and near-IR triggered release from polymeric nanoparticles. *J. Am. Chem. Soc.* **2010**, 132, 9540-9542.

43. Tibbitt, M. W.; Kloxin, A. M.; Dyamenahalli, K. U.; Anseth, K. S. Controlled two-photon photodegradation of PEG hydrogels to study and manipulate subcellular interactions on soft materials. *Soft Matter.* **2010**, 6, 5100-5108.

44. Jay, S. M.; Saltzman, W. M. Shining light on a new class of hydrogels. *Nat. Biotechnol.* **2009**, 27, 543.

45. Shigenaga, A.; Yamamoto, J.; Sumikawa, Y.; Furuta, T.; Otaka, A. Development and photo-responsive peptide bond cleavage reaction of two-photon near-infrared excitation-responsive peptide. *Tetrahedron Lett.* **2010**, 51, 2868-2871.

46. Álvarez, M.; Best, A.; Pradhan ‐ Kadam, S.; Koynov, K.; Jonas, U.; Kreiter, M. Single ‐ Photon and Two ‐ Photon Induced Photocleavage for Monolayers of an Alkyltriethoxysilane with a Photoprotected Carboxylic Ester. *Adv. Mater.* **2008**, 20, 4563-4567.

47. Aujard, I.; Benbrahim, C.; Gouget, M.; Ruel, O.; Baudin, J. B.; Neveu, P.; Jullien, L. o ‐ Nitrobenzyl Photolabile Protecting Groups with Red ‐ Shifted Absorption: Syntheses and Uncaging Cross ‐ Sections for One ‐ and Two ‐ Photon Excitation. *Chem. Eur. J.* **2006**, 12, 6865-6879.

48. Wu, S.; Butt, H. J. Near ‐ infrared ‐ sensitive materials based on upconverting nanoparticles. *Adv. Mater.* **2016**, 28, 1208-1226.

49. Zhu, X.; Su, Q.; Feng, W.; Li, F. Anti-Stokes shift luminescent materials for bio-applications. *Chem. Soc. Rev.* **2017**, 46, 1025-1039.

50. Jalani, G.; Tam, V.; Vetrone, F.; Cerruti, M. Seeing, targeting and delivering with

upconverting nanoparticles. *J. Am. Chem. Soc.* **2018**, 140, 10923-10931.
51. Möller, N.; Rühling, A.; Lamping, S.; Hellwig, T.; Fallnich, C.; Ravoo, B. J.; Glorius, F. Stabilization of High Oxidation State Upconversion Nanoparticles by N‐Heterocyclic Carbenes. *Angew. Chem. Int. Ed.* **2017**, 56, 4356-4360.
52. Kunitake, T. Synthetic Bilayer Membranes: Molecular Design, Self‐Organization, and Application. *Angew. Chem. Int. Ed.* **1992**, 31, 709-726.
53. Segré, D.; Ben-Eli, D.; Deamer, D. W.; Lancet, D. The lipid world. *Origins Life Evol. Biosphere.* **2001**, 31, 119-145.
54. Liu, C.; Ewert, K. K.; Wang, N.; Li, Y.; Safinya, C. R.; Qiao, W. A multifunctional lipid that forms contrast-agent liposomes with dual-control release capabilities for precise MRI-guided drug delivery. *Biomaterials*, **2019**, 221: 119412.
55. Liu, Q.; Song, L.; Chen, S.; Gao, J.; Zhao, P.; Du, J. A superparamagnetic polymersome with extremely high T2 relaxivity for MRI and cancer-targeted drug delivery. *Biomaterials.* **2017**, 114, 23-33.
56. Lee, C.-C.; Chu, S.-T.; Ho, H.-C.; Lee, C.-C.; Hung, S.-K. Primary tumor volume calculation as a predictive factor of prognosis in nasopharyngeal carcinoma. *Acta oto-laryngol.* **2008**, 128, 93-97.
57. Sorensen, A. G.; Patel, S.; Harmath, C.; Bridges, S.; Synnott, J.; Sievers, A.; Yoon, Y.-H.; Lee, E. J.; Yang, M. C.; Lewis, R. F. Comparison of diameter and perimeter methods for tumor volume calculation. *J. Clin. Oncol.* **2001**, 19, 551-557.
58. Fischer, A. H.; Jacobson, K. A.; Rose, J.; Zeller, R. Hematoxylin and eosin staining of tissue and cell sections. *CSH. Protoc.* **2008**, pdb. prot4986.
59. Cardiff, R. D.; Miller, C. H.; Munn, R. J. Manual hematoxylin and eosin staining of mouse tissue sections. *CSH. Protoc.* **2014**, pdb. prot073411.
60. de Carvalho, H. F.; Taboga, S. R. Fluorescence and confocal laser scanning microscopy imaging of elastic fibers in hematoxylin-eosin stained sections. *Histochem. Cell Biol.* **1996**, 106, 587-592.
61. Lammers, T.; Subr, V.; Ulbrich, K.; Peschke, P.; Huber, P. E.; Hennink, W. E.; Storm, G. Simultaneous delivery of doxorubicin and gemcitabine to tumors in vivo using prototypic polymeric drug carriers. *Biomaterials.* **2009**, 30, 3466-3475.
62. Wang, J.-k.; Zhou, Y.-y.; Guo, S.-j.; Wang, Y.-y.; Nie, C.-j.; Wang, H.-l.; Wang, J.-l.; Zhao, Y.; Li, X.-y.; Chen, X.-j. Cetuximab conjugated and doxorubicin loaded silica nanoparticles for tumor-targeting and tumor microenvironment responsive binary drug delivery of liver cancer therapy. *Mat. Sci. Eng. C.* **2017**, 76, 944-950.
63. Al-Jamal, K. T.; Al-Jamal, W. T.; Wang, J. T.-W.; Rubio, N.; Buddle, J.; Gathercole, D.; Zloh, M.; Kostarelos, K. Cationic poly-L-lysine dendrimer complexes doxorubicin and delays tumor growth in vitro and in vivo. *ACS nano.* **2013**, 7, 1905-1917.
64. Zhang, Y.; Cai, L.; Li, D.; Lao, Y.-H.; Liu, D.; Li, M.; Ding, J.; Chen, X. Tumor microenvironment-responsive hyaluronate-calcium carbonate hybrid nanoparticle enables effective chemotherapy for primary and advanced osteosarcomas. *Nano Res.* **2018**, 11, 4806-4822.
65. Wang, L.; Liu, Y.; Li, W.; Jiang, X.; Ji, Y.; Wu, X.; Xu, L.; Qiu, Y.; Zhao, K.; Wei, T. Selective targeting of gold nanorods at the mitochondria of cancer cells: implications for cancer therapy. *Nano Lett.* **2010**, 11, 772-780.

66. Edler, M.; Mayrbrugger, S.; Fian, A.; Trimmel, G.; Radl, S.; Kern, W.; Griesser, T. Wavelength selective refractive index modulation in a ROMP derived polymer bearing phenyl- and ortho-nitrobenzyl ester groups. *J. Mater. Chem. C.* **2013**, 1, 3931-3938.
67. Jiang, X.; Lavender, C. A.; Woodcock, J. W.; Zhao, B. Multiple micellization and dissociation transitions of thermo-and light-sensitive poly (ethylene oxide)-b-poly (ethoxytri (ethylene glycol) acrylate-co-o-nitrobenzyl acrylate) in water. *Macromolecules.* **2008**, 41, 2632-2643.
68. Klinger, D.; Landfester, K. Dual stimuli-responsive poly (2-hydroxyethyl methacrylate-co-methacrylic acid) microgels based on photo-cleavable cross-linkers: pH-dependent swelling and light-induced degradation. *Macromolecules.* **2011**, 44, 9758-9772.
69. Israelachvili, J. N.; Mitchell, D. J.; Ninham, B. W. Theory of self-assembly of hydrocarbon amphiphiles into micelles and bilayers. *Journal of the Chemical Society, Faraday Transactions 2: Molecular and Chemical Physics.* **1976**, 72, 1525-1568.
70. Israelachvili, J., In; Burlington, MA: Academic Press: 2011.
71. Suarasan, S.; Focsan, M.; Potara, M.; Soritau, O.; Florea, A.; Maniu, D.; Astilean, S. Doxorubicin-incorporated nanotherapeutic delivery system based on gelatin-coated gold nanoparticles: formulation, drug release, and multimodal imaging of cellular internalization. *ACS Appl. Mat. Interfaces.* **2016**, 8, 22900-22913.
72. Fang, Z.; Bhandari, B. Encapsulation of polyphenols–a review. *Trends Food Sci. Tech.* **2010**, 21, 510-523.
73. Watwe, R. M.; Bellare, J. R. Manufacture of liposomes: a review. *Curr. Sci.* **1995**, 715-724.
74. Fritze, A.; Hens, F.; Kimpfler, A.; Schubert, R.; Peschka-Süss, R. Remote loading of doxorubicin into liposomes driven by a transmembrane phosphate gradient. *BBA-Biomembranes.* **2006**, 1758(10): 1633-1640.
75. Li, X.; Hirsh, D. J.; Cabral-Lilly, D.; Zirkel, A.; Gruner, S. M.; Janoff, A. S.; Perkins, W. R.. Doxorubicin physical state in solution and inside liposomes loaded via a pH gradient. *BBA-Biomembranes*. **1998**, 1415(1): 23-40.
76. Barenholz, Y. C. Doxil®—the first FDA-approved nano-drug: lessons learned. *J. Control. Release.* **2012**, 160(2): 117-134.
77. Franken, L. E.; Boekema, E. J.; Stuart, M. C. A. Transmission electron microscopy as a tool for the characterization of soft materials: application and interpretation. *Adv. Sci.* **2017**, 4(5): 1600476.
78. Lengyel, J. S.; Milne, J. L. S.; Subramaniam, S. Electron tomography in nanoparticle imaging and analysis. *Nanomedicine*. **2008**, 3(1):125-131.
79. Ross, J. F.; Chaudhuri, P. K.; Ratnam, M. Differential regulation of folate receptor isoforms in normal and malignant tissues in vivo and in established cell lines. Physiologic and clinical implications. *Cancer.* **1994**, 73, 2432-2443.
80. Zhao, H.; Yung, L. Y. L. Selectivity of folate conjugated polymer micelles against different tumor cells. *Int. J. Pharm.* **2008**, 349, 256-268.